# The MODY-associated TALK-1 L114P mutation causes islet α-cell overactivity and β-cell inactivity resulting in transient neonatal diabetes and glucose dyshomeostasis in adults

Arya Y. Nakhe[1], Prasanna K. Dadi[1], Jinsun Kim[1,2], Shristi Shrestha[3], Jean-Philippe Cartailler[3], Leesa Sampson[3], Mark A. Magnuson[1,3,4], and David A. Jacobson[1]

[1]Department of Molecular Physiology and Biophysics, Vanderbilt University, Nashville, TN 37232, USA

[2]Department of Chemistry, Vanderbilt University, Nashville, TN 37232, USA

[3]Center for Stem Cell Biology, Vanderbilt University, Nashville, TN 37232, USA

[4]Department of Cell and Developmental Biology, Vanderbilt University, Nashville, TN 37232, USA

*Corresponding author: David A. Jacobson
Email: david.a.jacobson@vanderbilt.edu. Phone: (615) 875-7655.
Department of Molecular Physiology and Biophysics, Vanderbilt University, 7425B MRBIV, 2213 Garland Ave., Nashville, TN, 37232-0615, USA.

## Abstract

A strong association of the gain-of-function mutation in the TALK-1 $K^+$ channel (p.L114P) with maturity-onset diabetes of the young (MODY) was recently reported in two distinct families. TALK-1 is a key regulator of β-cell electrical activity and glucose-stimulated insulin secretion (GSIS). *KCNK16*, the gene that encodes TALK-1, is the most abundant and β-cell–restricted $K^+$ channel transcript and *KCNK16* locus is strongly associated to type-2 diabetes. To investigate the impact of TALK-1-L114P on glucose homeostasis and confirm its association with MODY, a mouse model containing the *Kcnk16* L114P mutation was generated. Heterozygous and homozygous *Kcnk16* L114P mice exhibit increased neonatal lethality in the C57BL/6J and the CD-1(ICR) genetic background, respectively. Lethality is likely a result of severe hyperglycemia observed in the homozygous *Kcnk16* L114P neonates due to lack of GSIS and can be reduced with insulin treatment. TALK-1-L114P drastically increases whole-cell β-cell $K^+$ currents resulting in blunted glucose-stimulated $Ca^{2+}$ entry and a complete loss of glucose-induced $Ca^{2+}$ oscillations. Thus, adult *Kcnk16* L114P mice have reduced GSIS and plasma insulin levels, which significantly impairs glucose homeostasis. Taken together, this study shows that the MODY-associated TALK-1-L114P mutation disrupts glucose homeostasis in adult mice resembling a MODY phenotype and causes neonatal lethality by altering islet hormone secretion during development. These data strongly suggest that TALK-1 is an islet-restricted target for the treatment for diabetes.

## Introduction

Maturity Onset Diabetes of the Young (MODY) is a collection of monogenic forms of early-onset familial diabetes resulting from β-cell dysfunction. To date, mutations in 15 genes involved in β-cell development and function have been associated with MODY(1). Monogenic diabetes cases account for approximately 1%- 5% of the total diabetic patient population(2, 3). However, as the phenotype of MODY overlaps with other forms of diabetes, many patients are misdiagnosed(4, 5). Data from monogenic diabetes registries also suggests that in the US, ~70% of the registered cases (2680/3800) still do not have a known genetic cause, and similarly many patients in the UK (~50%) with monogenic diabetes have MODY-causing mutations that remain to be determined(6, 7). Additionally, some MODY-associated mutations are only reported in single families, and thus require genetic and mechanistic confirmation (8, 9). We recently identified a mutation in *KCNK16*, the gene encoding TALK-1 channels (p. TALK-1 L114P), which co-segregates with MODY in a four-generation family(10). Importantly, this mutation causes a gain-of-function (GOF) in TALK-1 channel activity. As *KCNK16* is the most islet-restricted and abundant β-cell $K^+$ channel transcript, the TALK-1 L114P mutation is likely to perturb β-cell function and cause MODY(11, 12). This was further strengthened by a recent report of a Japanese family with the identical *KCNK16* mutation (p. TALK-1 L114P) segregating with MODY(13). Thus, it is important to determine the mechanistic underpinnings of how this specific mutation in TALK-1 impacts islet function and results in glucose dyshomeostasis.

TALK-1 is a key regulator of β-cell membrane potential ($V_m$), glucose-stimulated $Ca^{2+}$ influx and insulin secretion(14). A non-synonymous GOF polymorphism in *KCNK16* (rs1535500; p. TALK-1 A277E) is also associated with an increased risk for type-2 diabetes (T2D)(15, 16). Moreover, we recently determined that the MODY-associated TALK-1 L114P mutation results in a significant GOF in TALK-1 $K^+$ flux(10). Thus, there is strong genetic evidence that alterations in TALK-1 function (e.g., TALK-1 L114P and TALK-1 A277E) result in diabetic phenotypes. Interestingly, when heterologously expressed in β-cells, TALK-1 L114P almost completely inhibited glucose-stimulated membrane potential ($V_m$) depolarization and $Ca^{2+}$ influx in most β-cells. While these TALK-1 L114P-mediated drastic changes in electrical activity and $Ca^{2+}$ would be predicted to fully inhibit glucose-stimulated insulin secretion (GSIS), they only resulted in partial blunting of β-cell GSIS. However, this is consistent with TALK-1 L114P MODY patients that required low-dose insulin therapy which also suggested that this mutation does not fully suppress GSIS. This differs from previous studies showing that inhibition of β-cell $Ca^{2+}$ influx with either $K^+$ channel pharmacological activation or GOF mutations (e.g., $K_{ATP}$ R201H) results in complete inhibition of GSIS(17). Therefore, it is critical to determine if endogenous TALK-1 L114P expression also shows complete inhibition of β-cell $Ca^{2+}$ influx and how this impacts GSIS. Another potential mechanism for the modest impact of TALK-1 L114P on GSIS could be due to its function in other islet cells. For example, TALK-1 is also expressed in δ-cells where its activity limits somatostatin secretion(18). Because somatostatin exerts inhibitory tone on islet β- and α-cells, TALK-1 L114P mediated reductions in δ-cell somatostatin secretion would be predicted to increase both glucagon and insulin secretion. Due to the β-cell intrinsic role of TALK-1

L114P channels, the effect of somatostatin on GSIS might be limited, however it remains to be determined if the fasting hyperglycemia observed in *KCNK16*-MODY patients is due in part to elevated glucagon secretion.

The nature and severity of MODY phenotypes is dictated by how specific gene mutations affect β-cell function. $K_{ATP}$ is the only ion channel besides TALK-1 to be linked to MODY; this is due to mutations in genes encoding the $K_{ATP}$ channel complex (*KCNJ11* and *ABCC8*) or mutations in genes affecting ATP synthesis (e.g., glucokinase)(19, 20). Interestingly, MODY-associated mutations in *KCNJ11* and *ABCC8* have also been found to cause other diabetic phenotypes including permanent or transient neonatal diabetes, and late-onset diabetes(21, 22). Although the two families with TALK-1 L114P primarily exhibit a MODY phenotype, it remains to be determined if *KCNK16* mutations are associated with other diabetic phenotypes besides MODY. Indeed, it was originally predicted that GOF TALK-1 mutations could cause neonatal diabetes, however, the voltage dependence of activation of TALK-1 makes this less likely that GOF TALK-1 channels would be active at resting $V_m$ PMID:11263999. Thus, TALK-1 GOF would limit but not abolish glucose-stimulated insulin secretion (GSIS) during β-cell glucose-mediated $V_m$ depolarization and cause MODY. As $K_{ATP}$ channels show larger unitary conductance than TALK-1, and are active at resting $V_m$, severe GOF in $K_{ATP}$ channels strongly suppress β-cell $Ca^{2+}$ entry and GSIS (23, 24). The biophysical differences in $K_{ATP}$ and TALK-1 especially in the context of nucleotide-gating predict differences in their corresponding MODY phenotypes. The phenotypes of *KCNJ11*- and *ABCC8*-MODY are well characterized; however, with only two known *KCNK16*-MODY families, it remains to

be elucidated how endogenous TALK-1 L114P disrupts islet electrical activity and glucose homeostasis.

Here we developed a mouse model harboring the MODY-associated *Kcnk16* variant p. TALK-1 L114P to investigate the impact of this mutation on glucose homeostasis and confirm its association with MODY. Interestingly, we observe increased neonatal lethality in heterozygous and homozygous *Kcnk16* L114P mice in the C57BL/6J (B6) and the B6;CD-1(ICR) mixed genetic backgrounds, respectively, likely due to severe hyperglycemia and lack of GSIS. Whereas in adult mice, TALK-1-L114P blunts glucose-stimulated β-cell electrical activity, $Ca^{2+}$ handling, and GSIS, thus significantly impairing glucose tolerance. These data strongly suggest that alterations in TALK-1 activity can disrupt islet hormone secretion and glucose homeostasis. Importantly, this study further confirms that the TALK-1-L114P mutation results in a MODY phenotype, but additionally predicts that GOF TALK-1 mutations cause transient neonatal diabetes.

## Results

***Kcnk16* L114P neonates exhibit loss of glucose stimulated $Ca^{2+}$ entry and insulin secretion leading to transient neonatal hyperglycemia and death.** To confirm the association of TALK-1 L114P in causing MODY, a mouse model harboring the *Kcnk16* mutation was developed in the C57BL/6J background using CRISPR/spCas9 (B6 *Kcnk16* L114P; Figure 1A and supplemental figures 1A and 1B). Surprisingly, heterozygous *Kcnk16* L114P (L/P) mice exhibited neonatal lethality as indicated by extremely low number of *Kcnk16* L114P (L/P) mice at weaning (Figure 1B). To increase the likelihood of survival of neonates, B6 *Kcnk16* L114P (L/P) mice were crossed with outbred CD-1(ICR) mice resulting in a progeny in the mixed (50:50) background (B6;CD-1 *Kcnk16* L114P; Figure 1A). Intriguingly, in the mixed background, neonatal lethality was observed in the homozygous B6;CD-1 *Kcnk16* L114P (P/P) mice on ~post-natal day 4 (P4), but not in the heterozygous B6;CD-1 *Kcnk16* L114P (L/P) mice (Supplemental figure 1C). Lethality was likely independent of growth defects as body weight did not differ between genotypes (Supplemental figure 1D). To test if lethality occurs from GOF TALK-1 L114P mediated defect in neonatal islet function, we assessed glycemic control and insulin secretion on P4. Heterozygous and homozygous *Kcnk16* L114P neonates showed severe hyperglycemia and a concurrent reduction in plasma insulin levels in a gene-dosage dependent manner compared to the control littermates (WT) on P4 (Figures 1C and 1D, and supplemental figure 1E). Additionally, TALK-1 L114P mutation blunted GSIS in islets from heterozygous neonates and decreased it further in islets from homozygous neonates (Figures 1E and 1F). These changes in GSIS and glucose homeostasis are likely due to TALK-1 L114P mediated alteration in islet function and not islet mass as

pancreas weight was unchanged (Figure 1G and supplemental figure 1F). Furthermore, neonatal islet composition was unaltered except for a modest increase in the α-cell (glucagon+) area/islet in the *Kcnk16* L114P(L/P) pancreas (Figures 1H-J). The loss of GSIS can be explained by a complete lack of glucose-stimulated $Ca^{2+}$ entry in islets from *Kcnk16* L114P (L/P and P/P) neonates (Figures 1K-N). However, these islets exhibited KCl-mediated β-cell $V_m$ depolarization-induced $Ca^{2+}$ entry; this indicates that TALK-1 L114P channels hyperpolarize β-cell $V_m$, thereby overriding the effect of $K_{ATP}$ closure due to glucose metabolism and lead to insufficient GSIS and hyperglycemia. Importantly, insulin treatment (Glargine Lantus; 0.2U/Kg/day, once-daily subcutaneous injection) was able to extend the lifespan of *Kcnk16* L114P (P/P) neonates suggesting lethality results from hyperglycemia due to inadequate insulin secretion (Figure 1O).

**Adult *Kcnk16* L114P mice exhibit fasting hyperglycemia and glucose intolerance.** Because neonatal *Kcnk16* L114P (L/P) mice showed transient hyperglycemia, we next assessed if TALK-1 L114P impairs glucose homeostasis in young-adulthood. Male *Kcnk16* L114P (L/P) mice developed glucose intolerance as early as 11-weeks of age in the B6;CD-1 background and 8-weeks of age in the B6 background compared to their respective control littermates (data not shown). This defect in glucose homeostasis is maintained with age in the male *Kcnk16* L114P (L/P) mice (Figures 2A-C and supplemental figures 2A-C). Furthermore, male *Kcnk16* L114P (L/P) mice also exhibit fasting hyperglycemia indicating a likely non-β-cell-specific islet defect in this mouse model (Figure 2B). There were no body weight differences in males (Figure 2D). Interestingly, the female *Kcnk16* L114P (L/P) mice develop moderate glucose intolerance

compared to the controls (WT) in both B6 and B6;CD-1 genetic backgrounds (Figures 2E-G and supplemental figures 2D-F). Moreover, TALK-1 L114P mutation leads to greater body weight gain in females compared to the WT controls (Figure 2H); this increase is likely contributed by lean mass which might render a protective effect on glucose tolerance in *Kcnk16* L114P (L/P) females compared to their male counterparts (Supplemental figures 3A-F). The T2D-associated SNP in *KCNK16* (rs1535500) which causes GOF in TALK-1 activity, has shown a significant association with increased total cholesterol in a Han Chinese population (25). However, an increase in TALK-1 activity due to the *Kcnk16* L114P mutation did not affect plasma- and liver- triglyceride and cholesterol levels in mice (Supplemental figures 3G-J).

**Adult *Kcnk16* L114P mice show disrupted islet hormone secretion and islet composition.** We then tested if the TALK-1-L114P-mediated impairment in glucose homeostasis arises from defective islet function. Both male and female *Kcnk16* L114P (L/P) mice exhibited reduced plasma insulin levels compared to controls at 15 min and 30 min following an intraperitoneal glucose injection after a 4-hour fast (Figures 3A and 3B). Insulin sensitivity was not altered in the *Kcnk16* L114P (L/P) mice indicating that the reduction in glucose tolerance is primarily due to an islet secretion defect (Figure 3C). This was confirmed by in vitro GSIS and glucose-inhibition of glucagon secretion (GIGS) measurements (Figures 3D and 3E). Islets from *Kcnk16* L114P (L/P) mice exhibited reduced ability to secrete insulin in response to glucose and showed elevated glucagon secretion under low glucose (2 mM) and euglycemic (7 mM) conditions (Figures 3D and 3E). This indicates that the fasting hyperglycemia observed in male *Kcnk16* L114P (L/P)

mice (Figure 2B) is likely a result of the observed increase in glucagon secretion under fasting conditions. We next investigated if impaired islet hormone secretion results from changes in islet composition. Immunostaining analyses revealed an increase in glucagon-positive area/ islet and a concurrent modest reduction in insulin-positive area/ islet in *Kcnk16* L114P (L/P) pancreata (Figures 3F-J). Together, these results indicate that TALK-1 L114P mutation leads to disruptions in both islet composition and secretion giving rise to a MODY-like phenotype in adult mice.

***Kcnk16* L114P blunts β-cell glucose-stimulated electrical excitability and increases whole-cell K2P currents.** We used patch-clamp electrophysiology to test if the reduction in GSIS results from decreased β-cell electrical excitability due to a GOF in TALK-1 activity in *Kcnk16* L114P mouse islets. Perforated patch-clamp recordings revealed blunting of β-cell $V_m$ depolarization and loss of action potential firing in islets from *Kcnk16* L114P (L/P) mice (Figures 4A and 4B). The lack of islet $V_m$ depolarization and action potentials was in part a result of increased whole-cell K2P currents at depolarized $V_m$ (Figures 4C and 4D). However, TALK-1 L114P (L/P and P/P) channels did not show a massive increase at hyperpolarized β-cell membrane potentials under low and high glucose where these $K^+$ currents are typically active (Supplementary figures 4A and 4B). Notably, the heterologously expressed human TALK-1 L114P channels exhibited a drastic GOF (>300-fold)(10); this suggests the likelihood of unknown endogenous regulator(s) of TALK-1 in β-cells. It is also likely that recording conditions lead to poor isolation of the endogenous TALK-1 L114P currents. Thus, K2P currents were assessed by overexpressing mouse TALK-1 L114P channels in HEK293T cells under identical

recording conditions as the human TALK-1 L114P study. Indeed, overexpression of the mouse mutant channel results in large $K^+$ currents indicative of a similar GOF in mouse TALK-1 current as the human TALK-1 current due to the L114P mutation (Figures 4E and 4F).

***Kcnk16* L114P reduces glucose- and tolbutamide-stimulated $Ca^{2+}$ entry and augments $IP_3$-induced $[Ca^{2+}]_{ER}$ release.** β-cell $Ca^{2+}$ entry was monitored in response to increasing concentrations of glucose in islets from WT and *Kcnk16* L114P (L/P) mice to assess if TALK-1 L114P-mediated $V_m$ hyperpolarization reduces glucose-stimulated $Ca^{2+}$ influx (GSCI). TALK-1 L114P blunted islet GSCI in mice on both B6 and B6;CD-1 genetic backgrounds compared to WT controls (Figures 5A-F and supplemental figures 5A and 5B). However, islets from male *Kcnk16* L114P (L/P) mice showed a larger reduction in normalized $Ca^{2+}$ peak and normalized area under the curve responses compared to their controls than islets from female *Kcnk16* L114P (L/P) mice compared to their controls (Figures 5A-F). TALK-1 L114P channels did not affect the basal $Ca^{2+}$ levels at 2 mM G; however, the activity of these channels resulted in increased glucose-stimulated phase 0 response compared to controls (Supplemental figures 6A and 6B). This suggests a reduction in endoplasmic reticulum (ER) $Ca^{2+}$ ($[Ca^{2+}]_{ER}$) storage in *Kcnk16* L114P islets. Furthermore, *Kcnk16* L114P islets also showed a complete lack of glucose-stimulated $Ca^{2+}$ oscillations monitored at 9 mM G (Supplemental figures 6C and 6D). We then assessed if the reduction in GSCI results from TALK-1 L114P overactivity on the β-cell plasma membrane by monitoring tolbutamide-stimulated $V_m$ depolarization-induced $Ca^{2+}$ entry. TALK-1 L114P mediated β-cell $V_m$ hyperpolarization overrides the $V_m$

depolarization caused by $K_{ATP}$ closure by tolbutamide. Thus, *Kcnk16* L114P islets do not exhibit $Ca^{2+}$ entry in response to tolbutamide. Interestingly, islets from TALK-1 L114P mice showed equivalent KCl-stimulated $Ca^{2+}$ entry compared to control islets; this suggests that the loss of GSCI in the TALK-1 L114P islets occurs due to enhanced $K^+$ ion flux through GOF in TALK-1 activity (Figures 5G and 5H). Our previous studies showed that TALK-1 channels are functional on the ER membrane where they function to provide a $K^+$ countercurrent for $Ca^{2+}$ release from the ER lumen(26). Thus, we tested if TALK-1 L114P regulates $[Ca^{2+}]_{ER}$ homeostasis by stimulating $G_q$-signaling using acetylcholine which results in $IP_3$ generation and $IP_3$-induced $[Ca^{2+}]_{ER}$ release. Indeed, $IP_3$-induced $[Ca^{2+}]_{ER}$ release was enhanced in islets from *Kcnk16* L114P mice compared to controls suggesting GOF TALK-1 channels are localized to the ER membrane where they facilitate increased $Ca^{2+}$ release from the ER lumen (Figures 5I and 5J).

**TALK-1 L114P islets exhibit altered expression of genes involved in β-cell identity, function, ion channel activity, hormone activity, inflammatory signaling, and extracellular matrix interaction pathways.** Despite the loss of glucose-stimulated islet electrical activity and $Ca^{2+}$ entry, *Kcnk16* L114P mice do not exhibit a drastic reduction in GSIS and overt diabetes. Therefore, compensatory mechanisms such as the amplification pathway for insulin secretion might be altered in *Kcnk16* L114P islets PMID: 11078440. Moreover, prolonged hyperglycemia (although modest in this model), would also be predicted to result in long-term gene expression changes in *Kcnk16* L114P islets that alter β-cell function. Thus, gene expression differences between WT and *Kcnk16* L114P mouse islets were quantified with bulk-RNA sequencing and validated with qRT-

PCR (Figures 6 A-D). We observed increased expression of many genes which regulate $Ca^{2+}$-independent potentiation of insulin secretion such as *Adcy5*, *Creb5, Adcyap1, and Adcyap1r1*; genes that may promote $Ca^{2+}$-independent secretion from *Kcnk16* L114P islets(27, 28). Additionally, broad changes in ion channel activity genes (e.g., *Cacna1g, Cacng8, Scn5a, Pkd1l1, Kcnk2, Gabrg1*, and *Fxyd3*) may contribute to altered $Ca^{2+}$ handling in *Kcnk16* L114P islets. Reduced $Ca^{2+}$ entry in *Kcnk16* L114P islets results in decreased expression of genes previously shown to be elevated in chronically depolarized *Abcc8*$^{-/-}$ β-cells such as *Serpina7*, *Asb11*, *Sall1*, and *Aldh1a3* (Figure 6A) (29). Finally, several stress-associated, fibrosis-related, and inflammatory signaling pathway genes are upregulated in *Kcnk16* L114P islets likely due to prolonged hyperglycemic conditions. These include dedifferentiation markers *Sox4, Sox6, Sox9, Hk2, Vim,* and *Cd36*, extracellular matrix-interaction pathway genes *Col1a1*, *Col1a2*, *Col3a1*, *Col14a1*, *Col6a1*, *and Dcn*, and inflammatory signaling genes *Cxcl1*, *Ccl2*, *Ccl11*, *Ccl22*, *Tgfb2, Il33*, *and Il6* (30-35). The data show that *Kcnk16* L114P islets exhibit gene expression differences in many pathways. Taken together, this suggests that perturbed *Kcnk16* L114P islet intrinsic (e.g., $Ca^{2+}$ handling) and extrinsic (e.g., hyperglycemia) pathways result in direct as well as indirect disruption of islet function.

## Discussion

GOF in TALK-1 activity is associated with diabetic phenotypes, suggesting a causal role for overactive TALK-1 in islet dysfunction and diabetes progression. Utilizing a GOF model of TALK-1 (L114P) this study uncovered that disrupted β-cell and α-cell function resulted in glucose intolerance in adolescent mice confirming the association of the TALK-1 L114P mutation with MODY-like diabetes. Importantly, our data also revealed that TALK-1 L114P mutation can cause transient neonatal diabetes. This finding suggests that transient neonatal diabetic patients with unknown genetic diagnosis should be screened for mutations in *KCNK16.* Moreover, our data provides further genetic evidence that TALK-1 is a potentially novel therapeutic target for diabetes treatment. Specifically, in mice heterozygous for *Kcnk16* L114P mutation we observe neonatal hyperglycemia due to blunted GSIS, which can additionally result in neonatal death in mice homozygous for the mutant allele of *Kcnk16*. In young-adulthood, TALK-1 L114P causes glucose intolerance due to a reduction in GSIS mediated by enhanced β-cell $V_m$ hyperpolarization and reduced glucose-stimulated $Ca^{2+}$ entry. In addition to the β-cell intrinsic defect, the TALK-1 L114P mutation led to an increase in α-cell area fraction in islets and elevation of glucagon secretion under fasting conditions. Together these data highlight the crucial role of TALK-1 in β-cell function and glucose homeostasis and raises the possibility of TALK-1 inhibition as a druggable target for not only *KCNK16*-associated MODY but possibly for other forms of diabetes. Unlike the only other MODY-associated $K^+$ channelopathy (*KCNJ11* and *ABCC8* i.e., $K_{ATP}$ channel mutations), TALK-1 is not inhibited by sulfonylureas (14).

β-cell maturation and glucose-responsiveness of neonatal islets rapidly develops after birth and GSIS is required for efficient glucose uptake, which contributes to normal growth. Following birth, a shift to intermittent feeding and elevated plasma glucose requires an increase in β-cell insulin secretion for efficient nutrient absorption, as well as a suppression of insulin release during fasting to avoid hypoglycemia(36). Glucose-sensitivity in mouse β-cell $Ca^{2+}$ handling and insulin secretion develops over the first 4 postnatal days due to changes in β-cell metabolism, $K_{ATP}$ surface localization, and $Ca^{2+}$-dependent secretory machinery (37). Thus, mice expressing ATP-insensitive $K_{ATP}$ channels die shortly after birth due to hypoinsulinemia, severe hyperglycemia, and ketoacidosis (38). *Kcnk16* L114P mice show a similar phenotype, with neonatal islets showing a complete loss of GSCI, a drastic reduction in GSIS, and severe hyperglycemia by P5. Interestingly, TALK-1 L114P-mediated susceptibility to neonatal lethality was dependent on genetic diversity in mouse strains. Heterozygous *Kcnk16* L114P caused almost complete neonatal lethality in the B6 background but only hyperglycemia in the B6:CD-1 background, whereas homozygous *Kcnk16* L114P led to neonatal lethality in the B6:CD-1 mice. Although the neonatal glycemic data from the *Kcnk16* L114P families does not exist, it may be that neonatal lethality is not observed in affected individuals. However, it is interesting to note that all currently identified individuals carrying the *Kcnk16* L114P mutation are females (N=8) (10, 13). The importance of hypoinsulinemia causing neonatal diabetes and lethality in TALK-1 L114P mice was confirmed by insulin treatment which extended their lifespan. This resembles other monogenic forms of neonatal diabetes that require exogenous insulin treatment for survival (39). Indeed, it has been well established that insulin signaling is required for neonatal survival; for

example, a similar neonatal lethality phenotype was observed in mice without insulin receptors (*Insr*$^{-/-}$) where death results from hyperglycemia and diabetic ketoacidosis by P3 (40). Future studies are required to determine if TALK-1 GOF mutations result in human transient neonatal diabetes and are possibly followed by a MODY phenotype. Other monogenic diabetes mutations such as in genes encoding $K_{ATP}$ channels result in transient neonatal diabetes and diabetes remits later in life (41).

In adolescence, the timeline of development of MODY-like diabetes in the *Kcnk16* L114P (L/P) model is consistent with data from MODY patients. Similar to the timeline of disease progression in other MODY mouse models, *Kcnk16* L114P mice developed glucose intolerance during adolescence (~8 weeks in the B6 strain). The onset and severity of glucose intolerance in *Kcnk16* L114P mice also recapitulates the data from *Kcnk16* L114P MODY family probands, who were diagnosed at 11 and 15 years of age and displayed an abnormal oral glucose tolerance test (blood glucose:19 and 19.6 mmol/L, 2 hours after 75 g oral glucose bolus, respectively). The disease severity is more prominent in the inbred B6 strain compared to the mixed B6:CD-1 strain likely owing to the outbred characteristics and genetic diversity of the CD-1 strain, which recapitulates the diverse nature of MODY manifestation observed in human patients. Intriguingly, the patients from the Japanese *KCNK16* MODY family showed a greater insulin requirement compared to the patients from Australian *KCNK16* MODY family (10, 13). Interestingly, male *Kcnk16* L114P (L/P) mice exhibit more severe impairment in glucose homeostasis compared to female *Kcnk16* L114P (L/P) mice. A variety of factors could be at play here which could explain the observed sex-differences, including the female hormone 17β-estradiol (E2) which is critical for protection against glucolipotoxicity and oxidative stress(42).

Furthermore, for a given insulin action, comparing older men and women, women have higher insulin levels (43). Interestingly, GSCI in islets from female *Kcnk16* L114P mice is significantly greater than islets from male *Kcnk16* L114P mice, which would be predicted to lead to greater insulin secretion and lesser impairment in glucose tolerance in female *Kcnk16* L114P mice. Sexual dimorphism observed in GSCI could be mediated by differences in $Ca^{2+}$ handling or differences in TALK-1 function. Whether sex-differences exist in humans with TALK-1 L114P mutation remains to be determined as all affected individuals in both *KCNK16*-MODY (p. TALK-1 L114P) families were females. Neonatal lethality was more penetrant in male than female *Kcnk16* L114P (P/P) mice, thus, it will also be important to determine if *KCNK16*-MODY patients show neonatal phenotypes and display sexual dimorphism.

Similar to the proband from the human *KCNK16* L114P MODY family who showed elevated fasting blood glucose (~7mmol/L), *Kcnk16* L114P mice also exhibit fasting hyperglycemia. While this was predicted to be due to decreased insulin secretion, *Kcnk16* L114P islets showed equivalent insulin secretion under euglycemic conditions. However, these islets exhibited a significant elevation in fasting glucagon secretion which likely contributes to the fasting hyperglycemia. If TALK-1 L114P channels were expressed in α-cells, it would result in inhibition of α-cell $Ca^{2+}$ entry and glucagon secretion which supports previously described lack of TALK-1 protein expression in α-cells(18). This suggests that hyperglucagonemia in TALK-1 L114P islets is likely due to loss of inhibitory paracrine signaling. As insulin secretion does not change under fasting and euglycemic conditions, hyperglucagonemia might primarily be mediated by reduced somatostatin secretion. This is supported by a significant decrease in *Sst* expression in *Kcnk16* L114P

islets (Figure 6), which is likely due to reduced δ-cell secretion. Also, our previous data in global TALK-1 KO mice show higher somatostatin secretion and lower glucagon secretion, thus δ-cell TALK-1 L114P would be predicted to limit $Ca^{2+}$ influx and somatostatin secretion(18). Intriguingly, *Kcnk16* L114P islets additionally exhibit increased α-cell area fraction and a concurrent modest reduction in β-cell area fraction compared to control islets. These changes in islet composition in consistent with both T1D and T2D data showing increased α-cell: β-cell ratio (44, 45), which show elevated islet glucagon secretion. α-cell hyperplasia may result from increased activity/secretion, which is supported by other mediators of α-cell secretion (e.g., amino acids) that cause hyperplasia as well (46). However, loss of somatostatin also elevates α-cell secretion without altering α-cell mass(47). Moreover, the increased somatostatin and insulin secretion only result in reduced α-cell secretion without altering α-cell number. Thus, the exact mechanism of how TALK-1 L114P mediates increased α-cell number is not fully understood. Taken together, the *KcnK16* L114P mouse model shows disrupted glucagon and insulin secretion leading to fasting hyperglycemia and glucose intolerance, which provides confirmation that TALK-1 GOF mutations likely cause MODY.

One obstacle in determining how MODY-associated mutations result in β-cell dysfunction is the limited availability of primary islet tissue from MODY families. Due to this, the initial assessment of MODY-associated human TALK-1 L114P was performed in overexpression systems, which resulted in a drastic GOF. Similarly, overexpression of mouse *Kcnk16* L114P also leads to a significant GOF in TALK-1 activity (7.96-fold at -30 mV and 6.13-fold at 0 mV compared to TALK-1 WT). However, surprisingly β-cells from *Kcnk16* L114P (L/P and P/P) mice showed only a modest GOF in K2P currents. While

the slight increase in β-cell $K^+$ conductance from *Kcnk16* L114P mice would be predicted to partially alter islet excitability, these islets exhibit a complete loss of glucose-stimulated $V_m$ depolarization. This suggests that endogenous TALK-1 L114P polarizes plasma membrane potential, which is further supported by the robust KCl-induced $V_m$ depolarization and $Ca^{2+}$ entry observed in these islets. Because KCl shifts the reversal potential of $K^+$ channels to a more depolarized $V_m$, the constant $V_m$ hyperpolarization in TALK-1 L114P β-cells likely results from increased $K^+$ conductance through these channels. Yet, $K^+$ conductance in TALK-1 L114P β-cells was not significantly different at the hyperpolarized membrane potentials which these cells reside at under low and high glucose conditions. The recording conditions may lead to poor isolation of the endogenous TALK-1 L114P currents; however, overexpression of this mutant channel results in large $K^+$ currents under identical recording conditions. The $K^+$ conductance differences between heterologously versus endogenously expressed TALK-1 L114P channels points towards unidentified regulators of β-cell TALK-1 activity which could include endogenous ligands, protein interactions, and cellular localization of the channel. This is presumably not due to changes in TALK-1 protein levels because *Kcnk16* mRNA expression was not altered in control and *Kcnk16* (c. 337 T>C) islets. The subtle increase in β-cell $K^+$ conductance correlates with a modest MODY-like phenotype and likely allows for incomplete suppression of β-cell function. This is also observed in $K_{ATP}$-MODY, where channel activity is only modestly increased (21). Importantly, our study suggests that drastic TALK-1 GOF mutations only lead to modest β-cell $K^+$ conductance, which may explain why both families with TALK-1 MODY carry the same pore-domain mutation (L114P) in TALK-1. Additionally, it is likely that other less-severe GOF mutations in TALK-

1 (e.g., A277E) result in a milder phenotype such as T2D. Thus, it will be important to establish endogenous modulators of TALK-1 channels (WT and L114P) and how they contribute to β-cell dysfunction.

Suppression of glucose-stimulated electrical activity and $[Ca^{2+}]_c$ influx in *Kcnk16* L114P islets would be predicted to cause a greater reduction of GSIS than that observed. However, a few β-cells from *Kcnk16* L114P mice show modest $V_m$ depolarization; this resulted in a slight increase in $[Ca^{2+}]_c$ in response to glucose in a small subset of *Kcnk16* L114P islets, which could result in some GSIS. Interestingly, *Kcnk16* L114P islets also show reduced expression of *Fxyd3,* which encodes the auxiliary subunit of $Na^+/K^+$-ATPase and is a known negative regulator of GSIS in diabetic mice and humans (48). Other interesting gene expression differences that may increase GSIS in *Kcnk16* L114P islets include elevated expression (2.13-fold) of *Adcy5*, a $Ca^{2+}$-independent amplification pathway gene (27, 49). In humans, *Adcy5* depletion impairs glucose-dependent elevation of cAMP and associated insulin secretion, thus elevation in *Adcy5* expression would be predicted to increase GSIS via cAMP signaling(27). Expression levels of other cAMP-dependent pathway genes were also elevated in the *Kcnk16* L114P islets including *Creb5, Adcyap1,* and *Adcyap1r1(28)*. Moreover, *Slit1* and *Srgap3*, part of the SLIT-ROBO signaling which enhances GSIS, were upregulated (50). SLIT-ROBO signaling regulates not only $Ca^{2+}$ handling but also actin remodeling and thus, $Ca^{2+}$-independent signaling pathways. These gene expression changes suggest an increase in GSCI-independent mechanism(s) of insulin secretion may compensate for TALK-1 L114P-mediated loss of β-cell electrical activity and $Ca^{2+}$ entry.

Chronic hyperglycemia in diabetic patients and rodents results in islet dysfunction and destruction, thus hyperglycemia observed in the *Kcnk16* L114P mice could exacerbate β-cell failure. Glucotoxicity results in numerous islet transcriptome changes that in-part contribute to dysfunction. Similar to islets from diabetic patients, *Kcnk16* L114P islets exhibit an increase in *Aldob* (-fold) and *Nnat* (-fold) expression (51, 52). Additionally, *Pdk4* expression, a marker for the shift from utilization of glucose to fatty acids as the primary fuel source, is higher in *Kcnk16* L114P islets (2.78-fold). Elevated islet PDK4 expression is also observed in patients with T2D and in animals on a HFD (37). Although hyperglycemia would be predicted to negatively impact *Kcnk16* L114P islet function, no overt changes in β-cell mass were observed in these mice. This differs from mice with islets expressing $K_{ATP}$ GOF mutation, which show loss of β-cell mass (53). *Kcnk16* L114P may not cause a significant β-cell destruction because these mice show sufficient GSIS to prevent overt diabetes.

In summary, we showed that the MODY-associated TALK-1 L114P mutation elevates α-cell glucagon secretion under fasting and euglycemic conditions and blunts glucose-stimulated β-cell electrical activity and $Ca^{2+}$ entry leading to reduced insulin secretion. Together, elevated glucagon impairs fasting glycemia and reduced GSIS increases post-prandial glucose levels in adults. This phenotype was more prominent in the male *Kcnk16* L114P mice compared to the female *Kcnk16* L114P mice raising the question whether sex-differences translate in humans carrying this mutation. Surprisingly, the TALK-1 L114P mutation also resulted in severe transient neonatal diabetes which was lethal in the C57Bl/6J genetic background. Thus, these data hold potential clinical utility in that neonatal diabetes patients with unknown genetic linkage should be screened for

mutations in *KCNK16*. Together, these data strengthen the rationale for designing TALK-1 inhibitors for use as a therapeutic modality to treat diabetes.

## Methods

### Chemicals and reagents

All research materials were purchased from Thermo-Fisher (Waltham, MA, USA) or Sigma-Aldrich (St. Louis, MO, USA) unless otherwise specified.

### Mouse model generation and ethical approval

Neonatal mice used for the studies were postnatal day 0- to postnatal day 5-old, and adult mice used for the studies were 6- to 26-week-old, age- and gender- matched, bred in-house on a C57BL/6J or mixed C57BL/6J:CD-1(ICR) background. Animals were handled in compliance with guidelines approved by the Vanderbilt University Animal Care and Use Committee protocols (#M2200007-00). C57BL/6J.*Kcnk16*L114P mice (Kcnk16<em1Djaco>; MGI:7486559) were produced by the Vanderbilt Genome Editing Resource (Vanderbilt University, Nashville, TN. USA). Ribonucleoprotein complexes (RNPs) comprising chemically modified ctRNA (crRNA + tracrRNA) (50 ng/µl) and enhanced specificity SpCas9 protein (100 ng/µl), together with a 180-nucleotide single-stranded DNA (ssDNA) donor containing the *Kcnk16* L114P mutation (50 ng/ul), were obtained from MilliporeSigma (Burlington, MA, USA). These components were diluted in 10 mM Tris, 0.1 mM EDTA, pH 7.6, sourced from Teknova (Half Moon Bay, California, USA), and administered via pronuclear injection into C57BL/6J embryos acquired from mice from Jackson Labs (Bar Harbor, Maine, USA). crRNA sequence: 5'CCCTGCAGGTTATGGAAACC. 180 nucleotide ssDNA sequence: 5' CTAGAGCTGGTGGTTGGGGGTGGGAGCCAGTTCTGGGCTCTCTTTTCCCCGCATC TGCACACTCCCTTGCCCTGCAGGTTATGGGAATCCAGCCCCCAGCACGGAGGCAG GGCAGGTCTTCTGTGTCTTCTATGCTCTGATGGGGATCCCACTCAATGTGGTCTTC

CTCAACCATCTGGG. Mosaic F0 animals were screened for the L114P point mutation by standard PCR followed by a restriction fragment length polymorphism assay for a de novo HinfI site incorporated with silent mutations into the ssDNA. Animals carrying the desired mutation were confirmed by Sanger sequencing. Founder *Kcnk16* L114P (L/P) mouse was backcrossed onto the C57Bl/6J (B6) strain for 2 generations to obtain mice used for all studies performed on the B6 background. Additionally, B6 *Kcnk16* L114P (L/P) male mice were crossed with the CD-1 (ICR) strain to obtain F1 mice on a hybrid B6;CD-1 background to reduce the incidence of neonatal lethality. Crossings of heterozygous F1 B6;CD-1 *Kcnk16* L114P (L/P) mice were used for generating homozygous B6;CD-1 *Kcnk16* L114P (P/P) mice. For all the studies, littermates expressing the wildtype *Kcnk16* allele were used as controls (WT).

**Immunofluorescence**

Mouse pancreata were fixed in 4% paraformaldehyde and embedded with paraffin. Rehydrated 5-μm sections were stained with primary antibodies against insulin (dilution 1:1000; Dako, Santa Clara, CA, USA), somatostatin (dilution 1:300, GeneTex., Irvine, CA, USA), and glucagon (dilution 1:100; Abcam, Cambridge, United Kingdom) followed by secondary antibodies (dilution 1:500; anti-guinea pig Alexa Fluor 488, dilution 1:500; anti-mouse, Alexa Fluor 647, and dilution 1:500; anti-rabbit Alexa Fluor 546) as previously described(14). Sections were imaged either with a Nikon Eclipse TE2000-U microscope or fluorescent ScanScope (Aperio).

**Islet isolation**

Islets from neonatal mice were isolated on post-natal day 4 using the protocol described by Huang and Gu (54). Briefly, pancreata were isolated and broken into ~2mm pieces and digested in 200ul collagenase P (Roche, Basel, Switzerland). For digestion, the tube was left in a 37 °C incubator for up to 15 min and inverted two times every min. The lysate was spun at 500 x g for 10 s followed by three washes in RPMI, after which the islets were handpicked using a brightfield microscope.

Islets from adult mouse pancreata were isolated by collagenase P digestion and density gradient centrifugation as previously described(14). Following isolation, islets were either dispersed into clusters of cells or single cells with trituration in 0.005% trypsin or maintained as whole islets. Cells were cultured in RPMI 1640 supplemented with 15% FBS, 100IU/mL penicillin, 100mg/mL streptomycin, and 5.5 mM glucose (RPMI) in a humidified incubator at 37°C with an atmosphere of 95% air and 5% $CO_2$.

**Whole-cell K2P currents**

TALK-1 L114P currents were monitored using the whole-cell patch clamp technique using an Axopatch 200B amplifier with pCLAMP10 software. Digidata 1440 was used to digitize currents that were low-pass-filtered at 1 kHz and sampled at 10 kHz. Cells were washed with the extracellular buffer (modified Krebs-Ringer-HEPES buffer (KRHB)) containing (mM) 119.0 NaCl, 2.0 $CaCl_2$, 4.7 KCl, 25.0 HEPES, 1.2 MgSO4, 1.2 $KH_2PO_4$, and 11 mM glucose (pH 7.4 with NaOH). For isolation of K2P channel currents, $K_{ATP}$ channels were blocked with 100 μM tolbutamide, voltage-gated $K^+$ channels were blocked with 10 mM tetraethylammonium (TEA)(18, 26). Patch electrodes (3–5 MΩ) were backfilled with

intracellular solution (IC) containing (mM) 140.0 KCl, 1.0 $MgCl_2$, 10.0 EGTA, 10.0 HEPES, and 4.0 Mg-ATP (pH 7.25 with KOH). β-cell $V_m$ was ramped from -120 mV to +60 mV from a holding potential of -80 mV to generate K2P currents. Currents were measured in single β-cells from WT or *Kcnk16* L114P (L/P) mice, or in HEK293FT cells expressing either *Kcnk16* WT or mouse *Kcnk16* L114P channels. The whole-cell currents were analyzed using ClampFit (Molecular Devices) and Excel (Microsoft Corp., Redmond, WA, USA).

For K2P recordings in HEK293FT cells, the cells were grown to ~80% confluency in Dulbecco's Modified Eagle Media (DMEM) GlutaMax-I (Thermo Fisher Scientific) supplemented with 10% fetal bovine serum (FBS, Gibco), 100 IU·ml−1 penicillin (Gibco), and 100 mg·ml−1 streptomycin (Gibco) at 37°C, 5% CO2 in 100 mm tissue culture dishes. Cells were transfected with either pLV-CMV-m*Kcnk16*:P2A:EGFP or pLV-CMV-m*Kcnk16* L114P:P2A:EGFP plasmids using Lipofectamine 3000 and P3000 (Thermo Fisher Scientific) in antibiotic-free Opti-MEM™ I Reduced Serum Medium as per the manufacturer's protocol. K2P currents were only recorded from EGFP-positive cells.

**β-cell $V_m$ recordings**

β-cell $V_m$ was recorded by the perforated patch clamp technique using an Axopatch 200B amplifier with pCLAMP10 software. Whole islets were washed with KRHB with (mM) 119.0 NaCl, 2.0 $CaCl_2$, 4.7 KCl, 25.0 HEPES, 1.2 $MgSO_4$, 1.2 $KH_2PO_4$ (adjusted to pH 7.4 with NaOH) supplemented with 2 mM glucose and incubated in KRHB for 30 min at 37°C, 5% $CO_2$. Patch electrodes (3-5 MΩ) were backfilled with IC containing (mM) 140.0 KCl, 1.0 $MgCl_2$, and 5.0 HEPES (adjusted to pH 7.2 with KOH) supplemented with 20

μg/mL amphotericin B. Islets were perifused with KRHB supplemented with 2 mM glucose followed by KRHB with 10 mM glucose for monitoring $V_m$ changes. β-cell $V_m$ recordings were analyzed using ClampFit (Molecular Devices), Excel (Microsoft Corp., Redmond, WA, USA), and GraphPad Prism 8 (GraphPad Software Inc.).

**Intracellular $Ca^{2+}$ imaging**

On the day of experiment, islets were incubated for 30 min in RPMI supplemented with 2 μM Fura-2, AM (Molecular Probes) and 2 mM glucose. Fura-2, AM fluorescence (Ratio 340Ex/380Ex-535Em; $F_{340}/F_{380}$) was measured every 5 s as an indicator of intracellular $Ca^{2+}$ using a Nikon Eclipse Ti2 microscope equipped with a Photometrics Prime 95B 25mm sCMOS Camera(55). For $[Ca^{2+}]_c$ measurements, β-cell glucose-stimulated $Ca^{2+}$ influx was monitored in KRHB supplemented with the glucose concentrations specified in the figures. For $IP_3$-induced $[Ca^{2+}]_{ER}$ release measurements, islets were perifused in KRHB buffer containing 11 mM glucose, 100 μM diazoxide, without extracellular $Ca^{2+}$. Fura-2, AM fluorescence was monitored as an indicator of $IP_3$-mediated $[Ca^{2+}]_{ER}$ release upon stimulation of muscarinic receptor signaling by 100μM acetylcholine. For all measurements, the cells were perifused at a flow rate of 2 mL/min. Ex; Excitation wavelength (nm), Em; Emission wavelength (nm).

**Glucose homeostasis**

Chow-diet fed male and female mice underwent glucose tolerance test (GTT) and insulin tolerance test (ITT) as previously described(14). Briefly, mice were fasted for 4 h and then intraperitoneally (i.p.) injected with either 2 mg dextrose/g body weight for GTTs, or 0.75 UI human recombinant insulin/kg body weight for ITTs (catalog no. 12585014, Gibco™).

Tail glucose measurements were then taken at the indicated time points in the figures to measure glucose clearance.

**Body composition, tissue and plasma triglyceride and cholesterol measurements**

Measurement of lean tissue, fat and fluid in living mice was performed using Bruker's minispec Body Composition Analyzer. Plasma samples and livers were collected from ad-lib fed mice for triglyceride and cholesterol measurements. Total cholesterol and triglyceride was measured using standard enzymatic assays by the Vanderbilt University Medical Center Lipid Core.

**Plasma insulin, *in vitro* insulin, and glucagon secretion assays**

Plasma insulin from the neonates was measured on post-natal day 4 using Ultrasensitive Mouse Insulin ELISA kit (Catalog no. 10-1249-01). In adult mice, plasma insulin measurements were conducted in mice fasted for ~4 hours followed by intraperitoneal injection of 2mg dextrose/g body weight at 0-, 15-, and 30-min post injection. Tail blood samples were collected in Microvette® CB 300 K2 EDTA tubes (Catalog no. 16.444.100, Sarstedt) at the indicated time points and plasma insulin were measured using mouse ultrasensitive insulin ELISA kit (Mercodia Inc., Sweden). For *in vitro* insulin and glucagon secretion assays, islets were isolated from mice fed a standard chow diet and were incubated over-night in RPMI supplemented with 0.5mg/mL BSA. On the following day, islets were equilibrated in DMEM containing 0.5 mg/mL BSA, 0.5 mM $CaCl_2$ and 10.0 mM HEPES (DMEM*) supplemented with 10% FBS and 5.5 mM glucose for 1 h at 37°C, 5% $CO_2$. 20 islets/well were picked into 400 uL DMEM* without FBS at glucose concentrations specified in the figures in 24-well plate(s) and insulin or glucagon secretion

was measured over 1 h at 37°C and stored at -20°C until analysis. Insulin secretion was measured using mouse insulin ELISA kit (Catalog no. 10-1247-01, Mercodia Inc, Sweden) and glucagon secretion was measured using the mouse glucagon ELISA kit (and 10-1281-01, Mercodia Inc, Sweden).

**Bulk-RNA sequencing**

RNA was isolated from islets from ~15-week-old male mice (WT and *Kcnk16* L114P (L/P)) using Maxwell® 16 LEV simplyRNA Purification Kits (Catalog no. AS1280, Promega, USA). RNA integrity was analyzed using an Agilent 2100 Bioanalyzer, and only those samples with an RNA integrity number of seven or above were used. An Illumina NovaSeq 6000 instrument was used to produce paired-end, 150-nucleotide reads for each RNA sample. Paired-end RNA sequencing reads (150bp long) were trimmed and filtered for quality using Trimgalore v0.6.7(56). Trimmed reads were aligned and counted using Spliced Transcripts Alignment to a Reference (STAR) (57) v2.7.9a with the –quantMode GeneCounts parameter against the mm10 mouse genome and GENCODE comprehensive gene annotations (Release M23). ~178 million uniquely mapped reads were acquired per sample. DESeq2 package v1.34.0 (58) was used to perform normalization and downstream differential expression. Features counted fewer than 5 times across at least 3 samples were removed. Freezing condition of the samples and sequencing batch was included as batch factor in DESeq2 design to increase the sensitivity for finding differences between *Kcnk16* L114P v/s WT samples. Gene enrichment analysis implemented from Gene Ontology was applied using the clusterProfiler v4.2.2 package in R. Annotated gene sets GO was sourced from Genome wide annotation for Mouse (Carlson M (2019). org.Mm.eg.db: Genome wide annotation

for Mouse. R package version 3.8.2.). For GO, genes significantly up- or downregulated in different conditions were used as input. False discovery rate-adjusted P value < 0.05 and log2 fold change >1 was used to define differentially expressed genes.

**Quantitative PCR**

RNA was isolated from islets from 15-week-old, chow diet fed mice using Maxwell® 16 LEV simplyRNA Purification Kits (Catalog no. AS1280, Promega, USA). Reverse transcription was performed using a SuperScript™ IV First-Strand Synthesis System (Catalog no. 18091050, Invitrogen, Waltham, MA, USA). 20 ng cDNA was used for real-time qPCR reactions with KAPA SYBR FAST qPCR Kit (Catalog no. KK4618, Roche, Basel, Switzerland) using a CFX Opus Real-Time PCR System (Bio-Rad Laboratories). Primers used for qRT-PCR are listed in Supplemental table 1.

**Statistical Analysis**

Functional data were analyzed using Axon Clampfit (Molecular Devices), GraphPad Prism 8 (GraphPad Software Inc.), or Excel (Microsoft Corp., Redmond, WA, USA) and presented as mean ± standard error (SE) for the specified number of samples (N). Statistical significance was determined using two-tailed *t*-tests, one-way ANOVA, or two-way ANOVA as appropriate. P-value ≤0.05 was considered statistically significant.

## Acknowledgements

The *Kcnk16* L114P mouse model was developed by the Vanderbilt Genome Editing Resource Core (RRID:SCR018826) which is supported by the Diabetes Research and Training Center Grant (DK020593), and the Cancer Center Support Grant (CA68485), and the Vanderbilt Center for Stem Cell Biology. Paraffin-embedded pancreata were prepared and processed by The Vanderbilt Translational Pathology Shared Resource (2P30 CA068485-14). Immunostaining slide scanning was performed using the Islet and Pancreas Analysis (IPA) Core supported by the Vanderbilt Diabetes Research Center (DRTC; NIH grant DK20593). Analysis of the bulk RNA-Seq data was performed by Creative Data Solutions, part of the Vanderbilt Center for Stem Cell Biology. Body composition measurements were performed at the Vanderbilt Mouse Metabolic Phenotyping Center which is supported by the NIH grant 5U2CDK059637. Triglyceride and cholesterol measurements were performed by the Vanderbilt University Medical Center Lipid Core supported by the NIH DRTC grant DK020593. Research in the laboratory of DAJ was supported by NIH grants R01DK097392, R01DK129340, and R01DK115620. A few illustrations were created using BioRender.com.

## Author contributions

DAJ and AYN conceived the project. AYN, PKD, JK, SS, and JP conducted the experiments and/or analyzed/reviewed the data. LS and MAM developed the mouse model. AYN, SS, JP, LS, MAM and DAJ wrote and/or edited the manuscript.

**Declaration of interests:** All authors declare no competing interests.

## References


1. Broome DT, Pantalone KM, Kashyap SR, and Philipson LH. Approach to the Patient with MODY-Monogenic Diabetes. *J Clin Endocrinol Metab.* 2021;106(1):237-50.
2. Kavvoura FK, and Owen KR. Maturity onset diabetes of the young: clinical characteristics, diagnosis and management. *Pediatr Endocrinol Rev.* 2012;10(2):234-42.
3. Zhang H, Colclough K, Gloyn AL, and Pollin TI. Monogenic diabetes: a gateway to precision medicine in diabetes. *J Clin Invest.* 2021;131(3).
4. Shields BM, Hicks S, Shepherd MH, Colclough K, Hattersley AT, and Ellard S. Maturity-onset diabetes of the young (MODY): how many cases are we missing? *Diabetologia.* 2010;53(12):2504-8.
5. Greeley SAW, Polak M, Njolstad PR, Barbetti F, Williams R, Castano L, et al. ISPAD Clinical Practice Consensus Guidelines 2022: The diagnosis and management of monogenic diabetes in children and adolescents. *Pediatr Diabetes.* 2022;23(8):1188-211.
6. Bowden TL, Letourneau-Freiberg LR, Kandasamy B, Sanyoura M, Tian P, Harris AG, et al. Insight on Diagnosis and Treatment From Over a Decade of Research Through the University of Chicago Monogenic Diabetes Registry. *Front Clin Diabetes Healthc.* 2021;2.
7. Shepherd M, Shields B, Hammersley S, Hudson M, McDonald TJ, Colclough K, et al. Systematic Population Screening, Using Biomarkers and Genetic Testing, Identifies 2.5% of the U.K. Pediatric Diabetes Population With Monogenic Diabetes. *Diabetes Care.* 2016;39(11):1879-88.
8. Yamagata K, Oda N, Kaisaki PJ, Menzel S, Furuta H, Vaxillaire M, et al. Mutations in the hepatocyte nuclear factor-1alpha gene in maturity-onset diabetes of the young (MODY3). *Nature.* 1996;384(6608):455-8.
9. Pearson ER, Pruhova S, Tack CJ, Johansen A, Castleden HA, Lumb PJ, et al. Molecular genetics and phenotypic characteristics of MODY caused by hepatocyte nuclear factor 4alpha mutations in a large European collection. *Diabetologia.* 2005;48(5):878-85.
10. Graff SM, Johnson SR, Leo PJ, Dadi PK, Dickerson MT, Nakhe AY, et al. A KCNK16 mutation causing TALK-1 gain of function is associated with maturity-onset diabetes of the young. *JCI Insight.* 2021;6(13).
11. Bramswig NC, Everett LJ, Schug J, Dorrell C, Liu C, Luo Y, et al. Epigenomic plasticity enables human pancreatic alpha to beta cell reprogramming. *J Clin Invest.* 2013;123(3):1275-84.
12. Blodgett DM, Nowosielska A, Afik S, Pechhold S, Cura AJ, Kennedy NJ, et al. Novel Observations From Next-Generation RNA Sequencing of Highly Purified Human Adult and Fetal Islet Cell Subsets. *Diabetes.* 2015;64(9):3172-81.
13. Katsuyuki Matsui KT, Shizuyo Nagai, Yoshihiro Maruo, Hisato Suzuki, Mamiko Yamada, and Kenjiro Kosaki. *International Meeting in Pediatric Endocrinology (IMPE) 2023*. Buenos Aires, Argentina: Bioscientifica; 2023.
14. Vierra NC, Dadi PK, Jeong I, Dickerson M, Powell DR, and Jacobson DA. Type 2 Diabetes-Associated K+ Channel TALK-1 Modulates beta-Cell Electrical Excitability, Second-Phase Insulin Secretion, and Glucose Homeostasis. *Diabetes.* 2015;64(11):3818-28.
15. Cho YS, Chen CH, Hu C, Long J, Ong RT, Sim X, et al. Meta-analysis of genome-wide association studies identifies eight new loci for type 2 diabetes in east Asians. *Nat Genet.* 2011;44(1):67-72.
16. Replication DIG, Meta-analysis C, Asian Genetic Epidemiology Network Type 2 Diabetes C, South Asian Type 2 Diabetes C, Mexican American Type 2 Diabetes C, Type 2 Diabetes Genetic Exploration by Nex-generation sequencing in muylti-Ethnic Samples C, et al. Genome-wide trans-

ancestry meta-analysis provides insight into the genetic architecture of type 2 diabetes susceptibility. *Nat Genet.* 2014;46(3):234-44.
17. Gloyn AL, Pearson ER, Antcliff JF, Proks P, Bruining GJ, Slingerland AS, et al. Activating mutations in the gene encoding the ATP-sensitive potassium-channel subunit Kir6.2 and permanent neonatal diabetes. *N Engl J Med.* 2004;350(18):1838-49.
18. Vierra NC, Dickerson MT, Jordan KL, Dadi PK, Katdare KA, Altman MK, et al. TALK-1 reduces delta-cell endoplasmic reticulum and cytoplasmic calcium levels limiting somatostatin secretion. *Mol Metab.* 2018;9:84-97.
19. Bonnefond A, Philippe J, Durand E, Dechaume A, Huyvaert M, Montagne L, et al. Whole-exome sequencing and high throughput genotyping identified KCNJ11 as the thirteenth MODY gene. *PLoS One.* 2012;7(6):e37423.
20. Huopio H, Otonkoski T, Vauhkonen I, Reimann F, Ashcroft FM, and Laakso M. A new subtype of autosomal dominant diabetes attributable to a mutation in the gene for sulfonylurea receptor 1. *Lancet.* 2003;361(9354):301-7.
21. Yorifuji T, Nagashima K, Kurokawa K, Kawai M, Oishi M, Akazawa Y, et al. The C42R mutation in the Kir6.2 (KCNJ11) gene as a cause of transient neonatal diabetes, childhood diabetes, or later-onset, apparently type 2 diabetes mellitus. *J Clin Endocrinol Metab.* 2005;90(6):3174-8.
22. Devaraja J, Elder C, and Scott A. Non classic presentations of a genetic mutation typically associated with transient neonatal diabetes. *Endocrinol Diabetes Metab Case Rep.* 2020;2020.
23. Rorsman P, and Ashcroft FM. Pancreatic beta-Cell Electrical Activity and Insulin Secretion: Of Mice and Men. *Physiol Rev.* 2018;98(1):117-214.
24. Kang D, and Kim D. Single-channel properties and pH sensitivity of two-pore domain K+ channels of the TALK family. *Biochem Biophys Res Commun.* 2004;315(4):836-44.
25. Permana S, Lukman H, Norahmawati E, Eka Puspita O, Faisal Moh Al Zein D, Kawamoto Y, et al. East Asian Genome-wide association study derived loci in relation to type 2 diabetes in the Han Chinese population. *Acta Biochim Pol.* 2019;66(2):679-86.
26. Vierra NC, Dadi PK, Milian SC, Dickerson MT, Jordan KL, Gilon P, et al. TALK-1 channels control beta cell endoplasmic reticulum Ca(2+) homeostasis. *Sci Signal.* 2017;10(497).
27. Hodson DJ, Mitchell RK, Marselli L, Pullen TJ, Gimeno Brias S, Semplici F, et al. ADCY5 couples glucose to insulin secretion in human islets. *Diabetes.* 2014;63(9):3009-21.
28. Jamen F, Puech R, Bockaert J, Brabet P, and Bertrand G. Pituitary adenylate cyclase-activating polypeptide receptors mediating insulin secretion in rodent pancreatic islets are coupled to adenylate cyclase but not to PLC. *Endocrinology.* 2002;143(4):1253-9.
29. Stancill JS, Cartailler JP, Clayton HW, O'Connor JT, Dickerson MT, Dadi PK, et al. Chronic beta-Cell Depolarization Impairs beta-Cell Identity by Disrupting a Network of Ca(2+)-Regulated Genes. *Diabetes.* 2017;66(8):2175-87.
30. Roefs MM, Carlotti F, Jones K, Wills H, Hamilton A, Verschoor M, et al. Increased vimentin in human alpha- and beta-cells in type 2 diabetes. *J Endocrinol.* 2017;233(3):217-27.
31. Puri S, Akiyama H, and Hebrok M. VHL-mediated disruption of Sox9 activity compromises beta-cell identity and results in diabetes mellitus. *Genes Dev.* 2013;27(23):2563-75.
32. Szabat M, Pourghaderi P, Soukhatcheva G, Verchere CB, Warnock GL, Piret JM, et al. Kinetics and genomic profiling of adult human and mouse beta-cell maturation. *Islets.* 2011;3(4):175-87.
33. Eguchi K, and Nagai R. Islet inflammation in type 2 diabetes and physiology. *J Clin Invest.* 2017;127(1):14-23.
34. Homo-Delarche F, Calderari S, Irminger JC, Gangnerau MN, Coulaud J, Rickenbach K, et al. Islet inflammation and fibrosis in a spontaneous model of type 2 diabetes, the GK rat. *Diabetes.* 2006;55(6):1625-33.

35. Hayden MR, and Sowers JR. Isletopathy in Type 2 diabetes mellitus: implications of islet RAS, islet fibrosis, islet amyloid, remodeling, and oxidative stress. *Antioxid Redox Signal.* 2007;9(7):891-910.
36. Helman A, Cangelosi AL, Davis JC, Pham Q, Rothman A, Faust AL, et al. A Nutrient-Sensing Transition at Birth Triggers Glucose-Responsive Insulin Secretion. *Cell Metab.* 2020;31(5):1004-16 e5.
37. West HL, Corbin KL, D'Angelo CV, Donovan LM, Jahan I, Gu G, et al. Postnatal maturation of calcium signaling in islets of Langerhans from neonatal mice. *Cell Calcium.* 2021;94:102339.
38. Koster JC, Marshall BA, Ensor N, Corbett JA, and Nichols CG. Targeted overactivity of beta cell K(ATP) channels induces profound neonatal diabetes. *Cell.* 2000;100(6):645-54.
39. Polak M, and Cave H. Neonatal diabetes mellitus: a disease linked to multiple mechanisms. *Orphanet J Rare Dis.* 2007;2:12.
40. Accili D, Drago J, Lee EJ, Johnson MD, Cool MH, Salvatore P, et al. Early neonatal death in mice homozygous for a null allele of the insulin receptor gene. *Nat Genet.* 1996;12(1):106-9.
41. Flanagan SE, Patch AM, Mackay DJ, Edghill EL, Gloyn AL, Robinson D, et al. Mutations in ATP-sensitive K+ channel genes cause transient neonatal diabetes and permanent diabetes in childhood or adulthood. *Diabetes.* 2007;56(7):1930-7.
42. Gannon M, Kulkarni RN, Tse HM, and Mauvais-Jarvis F. Sex differences underlying pancreatic islet biology and its dysfunction. *Mol Metab.* 2018;15:82-91.
43. Basu A, Dube S, and Basu R. Men Are from Mars, Women Are from Venus: Sex Differences in Insulin Action and Secretion. *Adv Exp Med Biol.* 2017;1043:53-64.
44. Li Z, Karlsson FA, and Sandler S. Islet loss and alpha cell expansion in type 1 diabetes induced by multiple low-dose streptozotocin administration in mice. *J Endocrinol.* 2000;165(1):93-9.
45. Yoon KH, Ko SH, Cho JH, Lee JM, Ahn YB, Song KH, et al. Selective beta-cell loss and alpha-cell expansion in patients with type 2 diabetes mellitus in Korea. *J Clin Endocrinol Metab.* 2003;88(5):2300-8.
46. Dean ED. A Primary Role for alpha-Cells as Amino Acid Sensors. *Diabetes.* 2020;69(4):542-9.
47. Hauge-Evans AC, King AJ, Carmignac D, Richardson CC, Robinson IC, Low MJ, et al. Somatostatin secreted by islet delta-cells fulfills multiple roles as a paracrine regulator of islet function. *Diabetes.* 2009;58(2):403-11.
48. Vallois D, Niederhauser G, Ibberson M, Nagaraj V, Marselli L, Marchetti P, et al. Gluco-incretins regulate beta-cell glucose competence by epigenetic silencing of Fxyd3 expression. *PLoS One.* 2014;9(7):e103277.
49. Kalwat MA, and Cobb MH. Mechanisms of the amplifying pathway of insulin secretion in the beta cell. *Pharmacol Ther.* 2017;179:17-30.
50. Yang YH, Manning Fox JE, Zhang KL, MacDonald PE, and Johnson JD. Intraislet SLIT-ROBO signaling is required for beta-cell survival and potentiates insulin secretion. *Proc Natl Acad Sci U S A.* 2013;110(41):16480-5.
51. Gerst F, Jaghutriz BA, Staiger H, Schulte AM, Lorza-Gil E, Kaiser G, et al. The Expression of Aldolase B in Islets Is Negatively Associated With Insulin Secretion in Humans. *J Clin Endocrinol Metab.* 2018;103(12):4373-83.
52. Millership SJ, Da Silva Xavier G, Choudhury AI, Bertazzo S, Chabosseau P, Pedroni SM, et al. Neuronatin regulates pancreatic beta cell insulin content and secretion. *J Clin Invest.* 2018;128(8):3369-81.
53. Shyr ZA, Wang Z, York NW, Nichols CG, and Remedi MS. The role of membrane excitability in pancreatic beta-cell glucotoxicity. *Sci Rep.* 2019;9(1):6952.
54. Huang C, and Gu G. Effective Isolation of Functional Islets from Neonatal Mouse Pancreas. *J Vis Exp.* 2017(119).

55. Zaborska KE, Dadi PK, Dickerson MT, Nakhe AY, Thorson AS, Schaub CM, et al. Lactate activation of alpha-cell KATP channels inhibits glucagon secretion by hyperpolarizing the membrane potential and reducing Ca(2+) entry. *Mol Metab.* 2020;42:101056.
56. Felix Krueger FJ, Phil Ewels, Ebrahim Afyounian, Michael Weinstein, Benjamin Schuster-Boeckler, Gert Hulselmans, sclamons. Zenodo; 2023.
57. Dobin A, Davis CA, Schlesinger F, Drenkow J, Zaleski C, Jha S, et al. STAR: ultrafast universal RNA-seq aligner. *Bioinformatics.* 2013;29(1):15-21.
58. Love MI, Huber W, and Anders S. Moderated estimation of fold change and dispersion for RNA-seq data with DESeq2. *Genome Biol.* 2014;15(12):550.

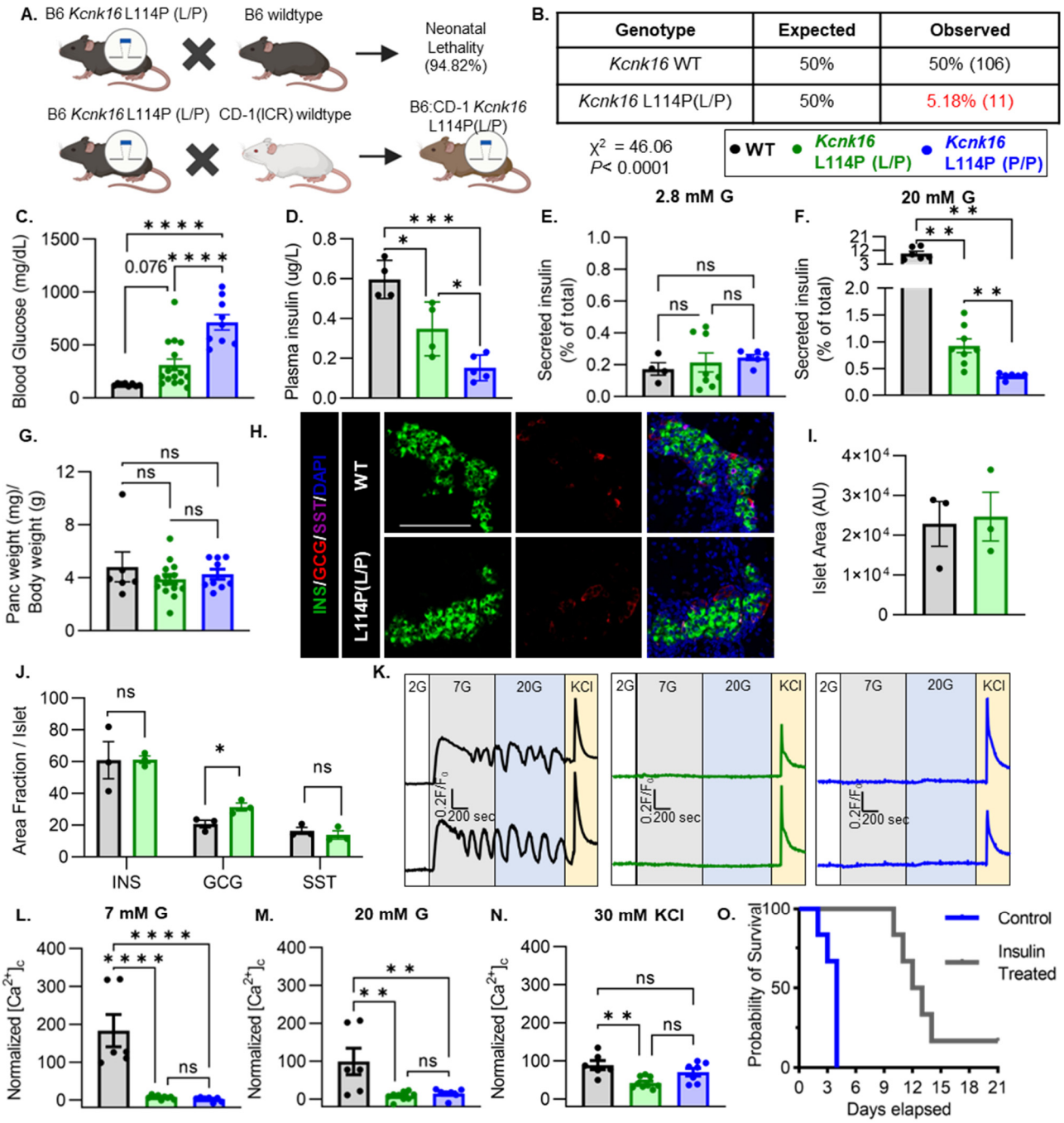


**Figure 1. *Kcnk16* L114P neonates exhibit loss of glucose stimulated $Ca^{2+}$ entry and insulin secretion leading to transient neonatal hyperglycemia and death. A.** Schematic of the *Kcnk16* L114P mouse line generation in the C57BL/6J background and the C57BL/6J:CD-1(ICR) mixed background. **B.** $\chi^2$ analysis of the F1 progeny from

C57BL/6J and heterozygous *Kcnk16* L114P (L/P) crossings genotyped at weaning on post-natal day 21 (P21). **C.** Blood glucose measurements of male wildtype (WT; black; N=8), heterozygous *Kcnk16* L114P (L/P; green; N=16), and homozygous *Kcnk16* L114P (P/P; blue; N=9) mice on P4. **D.** Plasma insulin measurements performed on P4 in WT (N=4), *Kcnk16* L114P (L/P; N=4), and *Kcnk16* L114P (P/P; N=5) neonates. **E. and F.** In-vitro glucose-stimulated insulin secretion from P4 mouse islets stimulated with 2.8 mM glucose (G) or 20 mM G, respectively (WT; N=4, *Kcnk16* L114P (L/P); N=8, and *Kcnk16* L114P (P/P); N=6). **G.** Pancreas weight/ body weight measurements of P4 male mice (WT; N=6, *Kcnk16* L114P (L/P); N=14, and *Kcnk16* L114P (P/P); N=9). **H.** Representative immunostaining images of pancreas sections from P0 WT and *Kcnk16* L114P (L/P) mice (N=3 mice/genotype), stained against insulin (INS; green), glucagon (GCG; red), somatostatin (SST; magenta), and Hoechst (blue); scale bar=100 µm. **I. and J.** Average islet area and area fraction of hormone staining per islet quantified using Fiji ImageJ software in P0 mouse pancreas sections. **K.** Representative glucose stimulated $Ca^{2+}$ influx traces from P4 mouse islets sequentially stimulated with 2 mM glucose (G), 7 mM G, 20 mM G, and 20 mM G with 30 mM KCl (WT; N=6, *Kcnk16* L114P (L/P); N=9, and *Kcnk16* L114P (P/P); N=7). **L-N.** Average area under the curve (AUC) analysis of normalized $Ca^{2+}$ during 7 mM G, 20 mM G, and 20 mM G+30 mM KCl stimulations. **O.** Survival curve for *Kcnk16* L114P (P/P) mice treated with (N=6) or without (N=6) insulin (Lantus insulin glargine; 0.2 U/kg/day) starting at P0 up until death or weaning. Data are presented as mean±SEM. Data were analyzed using student's t-test, one-way ANOVA, and two-way ANOVA as appropriate.

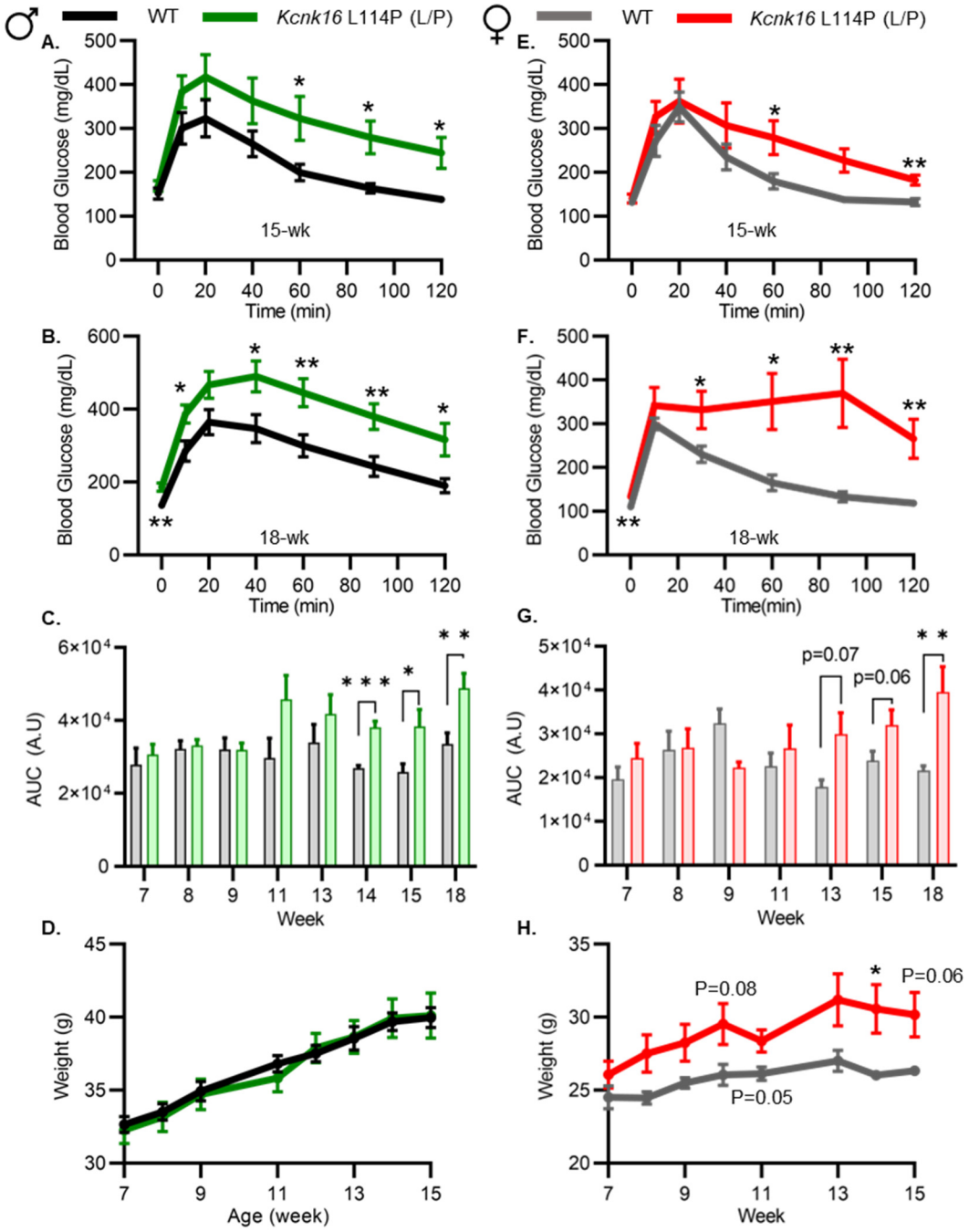


**Figure 2. Adult *Kcnk16* L114P mice exhibit fasting hyperglycemia and glucose intolerance. A.** and **B.** Intraperitoneal glucose tolerance test (i.p. GTT) performed in 15-week-old and 18-week-old male mice following a 4-hour fast in response to 2mg/g glucose injection (WT; black; N=8-10 and *Kcnk16* L114P (L/P); green; N=9-10). **C.**

Average AUC of the 2-hr GTT excursion profiles from ages 7 weeks up to 18 weeks in male mice. **D.** Weekly body weight measurements of male WT; N=5 mice and *Kcnk16* L114P (L/P); N=5 mice **E.** and **F.** I.P. GTT performed in 15-week-old and 18-week-old female mice following a 4-hour fast in response to 2mg/g glucose injection WT; N=9-11 and *Kcnk16* L114P (L/P); N=10-11. **G.** Average AUC of the 2-hr GTT excursion profiles from ages 7 weeks up to 18 weeks in female mice. **H.** Body weight measurements of female WT (black; N=4) and *Kcnk16* L114P (L/P; blue; N=5) mice. Data are presented as mean±SEM. Data were analyzed using student's t-test.

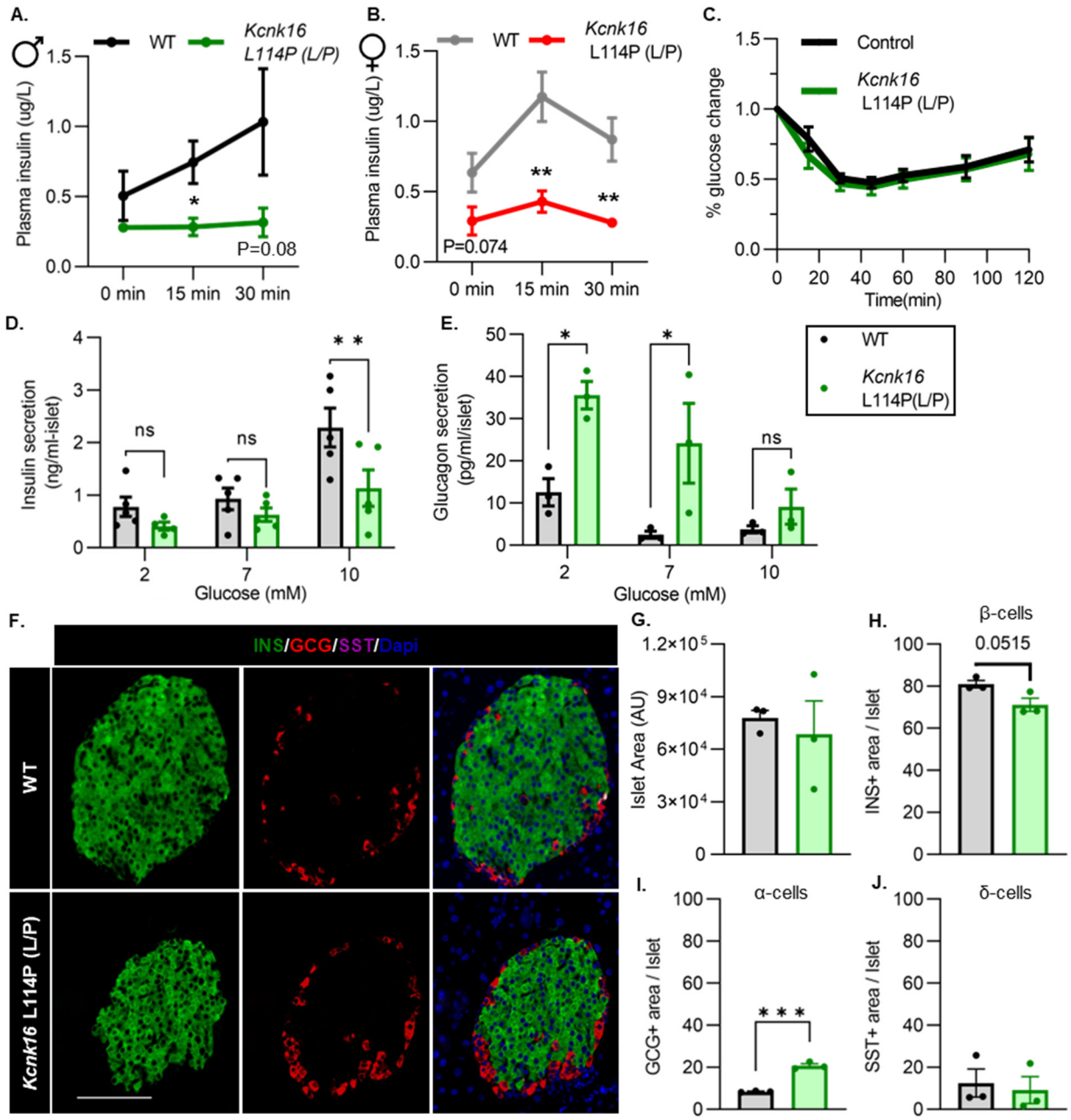


**Figure 3. Adult *Kcnk16* L114P mice show disrupted islet hormone secretion and islet composition. A. and B.** Plasma insulin levels in male (**A**) and female (**B**) WT and *Kcnk16* L114P(L/P) mice following a 4-hour fast at the indicated time points before and after a 2mg/g glucose injection. **c.** Glucose (%) change in response to an i.p. human insulin injection (0.75 UI/kg body weight) was measured as an indicator of insulin

sensitivity in WT and *Kcnk16* L114P male mice after a 4-hour fast. **D. and E.** In-vitro insulin secretion (N=5 mice/genotype) and glucagon secretion (N=3 mice/genotype) from male mice at the specified glucose concentrations **F.** Representative immunostaining images of pancreas sections from WT and *Kcnk16* L114P(L/P) male mice (N=3/genotype) stained against insulin (INS; green), glucagon (GCG; red), somatostatin (SST; magenta), and Hoechst (blue); scale bar = 100 μm. **G-J.** Average islet area and area of hormone staining/ islet for β-cells (INS), α-cells (GCG), and δ-cells (SST). Data are presented as mean±SEM. Data were analyzed using student's t-test or two-way ANOVA as appropriate.

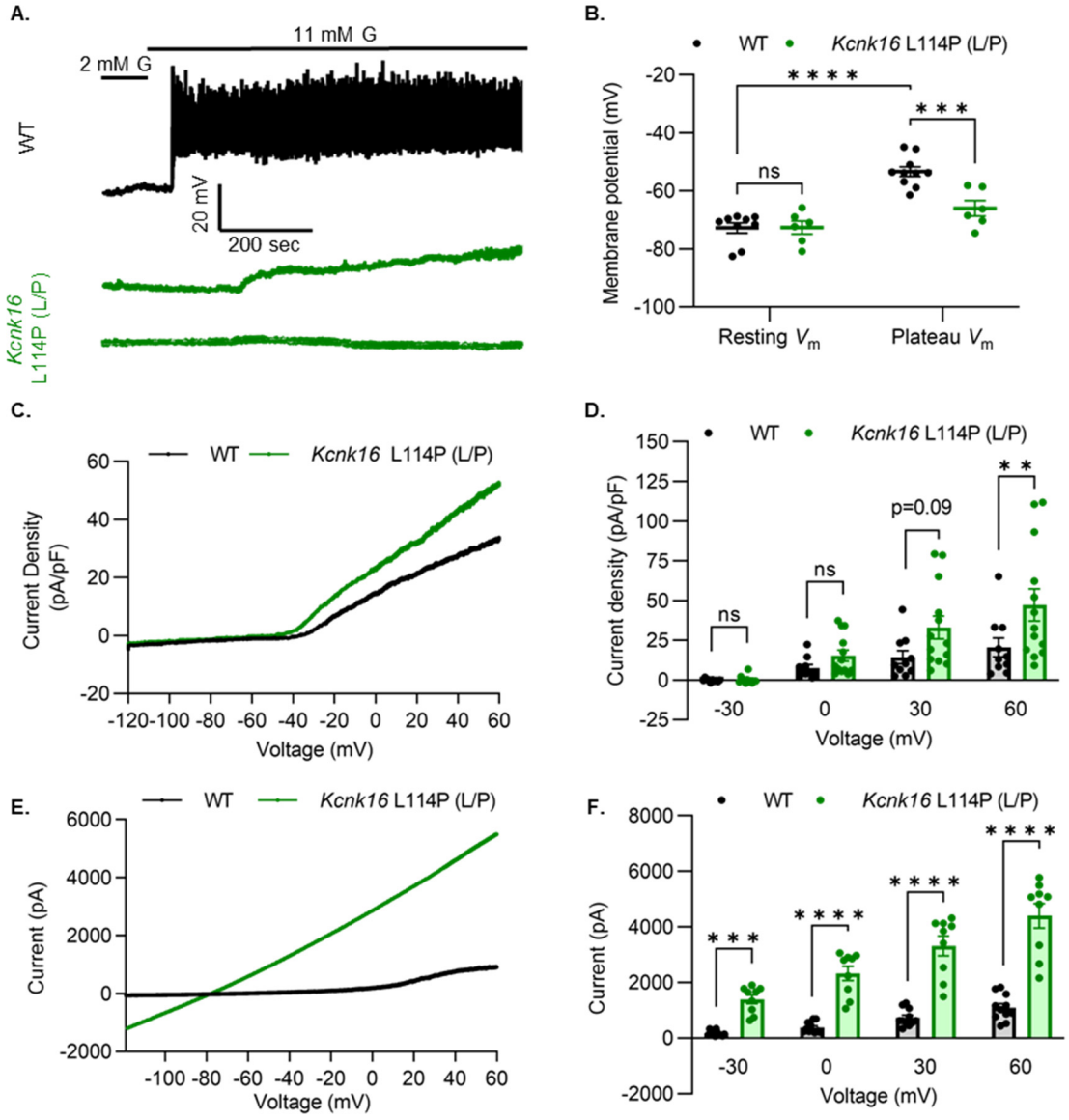


**Figure 4. *Kcnk16* L114P blunts β-cell glucose-stimulated electrical excitability and increases whole-cell K2P currents. A.** Representative perforated patch-clamp $V_m$ recordings in response to 2 mM G and 11 mM G in islets from WT and *Kcnk16* L114P(L/P) mice (N=6-10 islets from 5 mice/genotype). **B.** Average resting islet $V_m$ under 2 mM G and plateau islet $V_m$ at 11 mM G. **C.** Representative whole-cell K2P current density (pA/pF) recorded using a voltage ramp (-120 mV to +60 mV) at 11 mM G in β-cells from WT and *Kcnk16* L114P(L/P) mice. **D.** Average current density (pA/pF) at the specified

membrane voltages during the voltage ramp recordings shown in panel **C**. **(**N=9-13 cells/genotype). **E.** Representative whole-cell K2P current (pA) recorded using a voltage ramp (-120 mV to +60 mV) in 11 mM G in HEK293T cells expressing either *Kcnk16* WT or *Kcnk16* L114P(L/P). **F.** Average current (pA) at the specified membrane voltages during the voltage ramp recordings shown in panel E. (N=9-11 cells/ group). Data are presented as mean±SEM. Data were analyzed using two-way ANOVA.

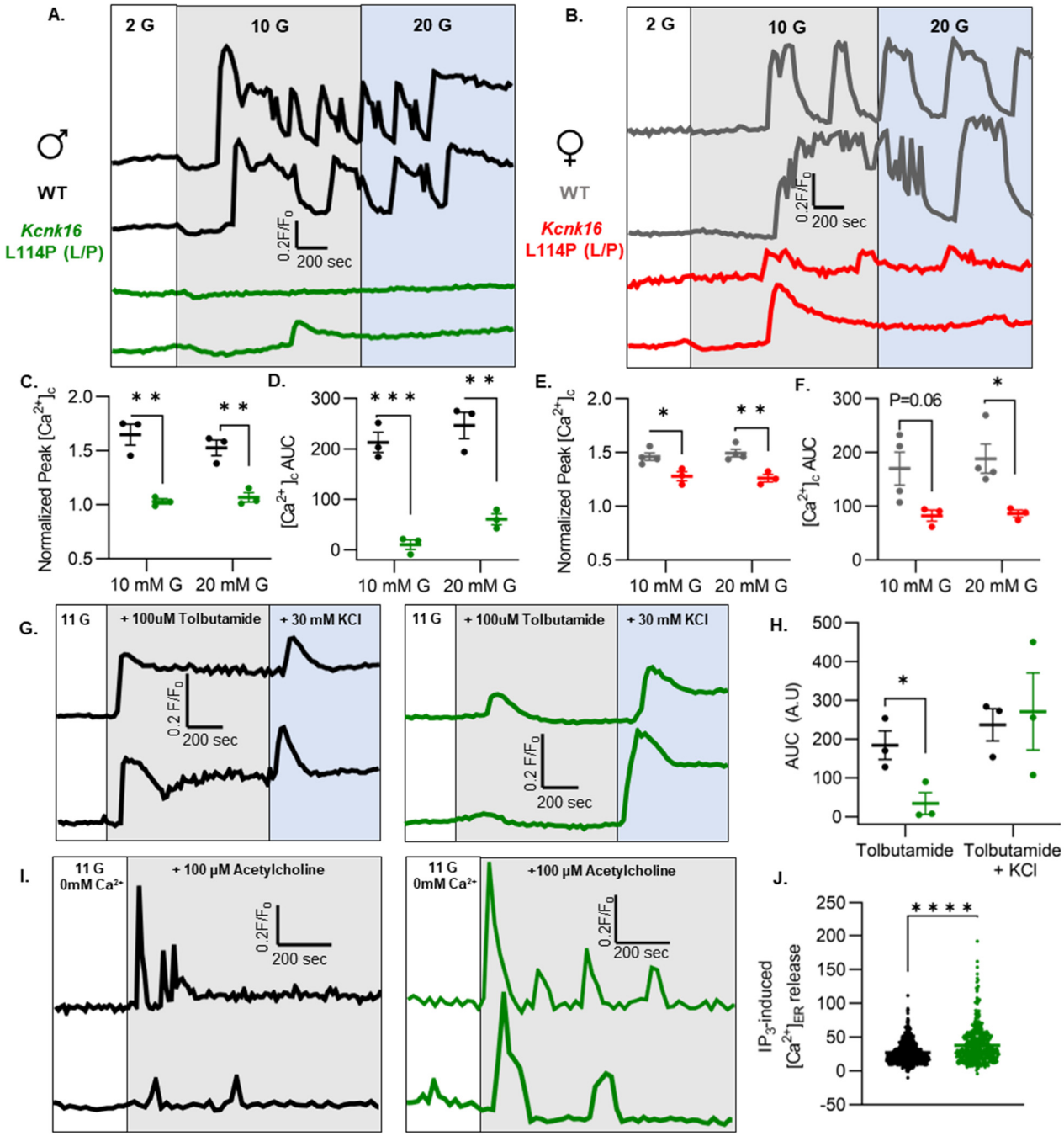


**Figure 5. *Kcnk16* L114P reduces glucose- and tolbutamide-stimulated islet $Ca^{2+}$ entry and augments $IP_3$-induced islet $[Ca^{2+}]_{ER}$ release. A. and B.** Representative $[Ca^{2+}]_c$ traces in islets from male (A) and female (B) WT and *Kcnk16* L114P(L/P) mice in response to 2 mM G, 10 mM G, and 20 mM G. **C-F.** Average normalized $Ca^{2+}$ peak (C.

and E.) and total AUC (D. and F.) in response to the indicated glucose concentrations in islets from male and female WT and *Kcnk16* L114P(L/P) mice (N=3-4/genotype). **G.** Representative $[Ca^{2+}]_c$ traces in islets from WT and *Kcnk16* L114P(L/P) male mice in response to 100 μM tolbutamide followed by 30 mM KCl stimulation. **H.** Average AUC of normalized $[Ca^{2+}]_c$ during 100 μM tolbutamide or 100 μM tolbutamide with 30 mM KCl stimulation (N=3 mice/genotype). **I**. Representative $[Ca^{2+}]_c$ traces in response to 100 μM acetylcholine in the absence of extracellular $Ca^{2+}$ in islets from male WT and *Kcnk16* L114P(L/P) mice. **J**. Average AUC of normalized $[Ca^{2+}]_c$ following 100 μM acetylcholine stimulated $[Ca^{2+}]_{ER}$ release (N=876 cells; WT, N=513 cells; *Kcnk16* L114P (L/P)). Data are presented as mean±SEM. Data were analyzed using student's t-test.

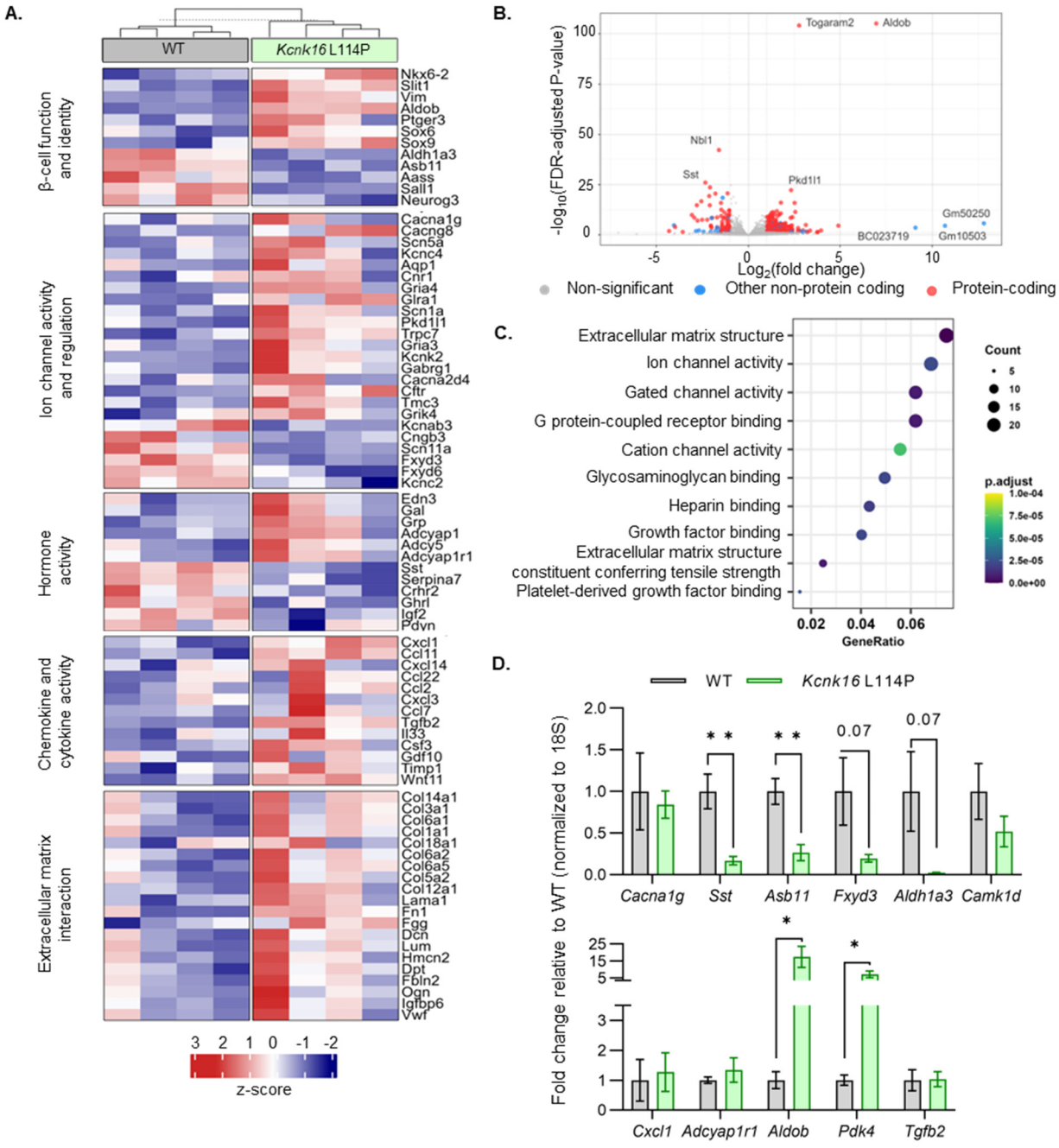


**Figure 6. *Kcnk16* L114P islets exhibit altered expression of genes involved in β-cell identity and function, ion channel activity, hormone activity, inflammatory signaling, and extracellular matrix interaction pathways. A.** Heatmap of a selected gene subsets showing differential gene expression in WT and *Kcnk16* L114P islets.

Normalized expression levels were scaled and centered by rows. **B.** Volcano plot displays genes differentially expressed between WT and *Kcnk16* L114P samples. Differentially expressed genes are defined by FDR <0.05 and log2FC (≥1). **C.** Dotplot represents the top 10 most significantly (FDR <0.05) altered Gene Ontology (Molecular Function). GeneRatio represent (count of enriched genes) / (count of genes in the GO term). The color represents FDR adjusted p-values and the size of the dot represents the number of genes that are significant from the experimental dataset. **D.** qRT-PCR validation of the gene expression differences in WT and *Kcnk16* L114P samples for the selected genes observed through bulk-sequencing.

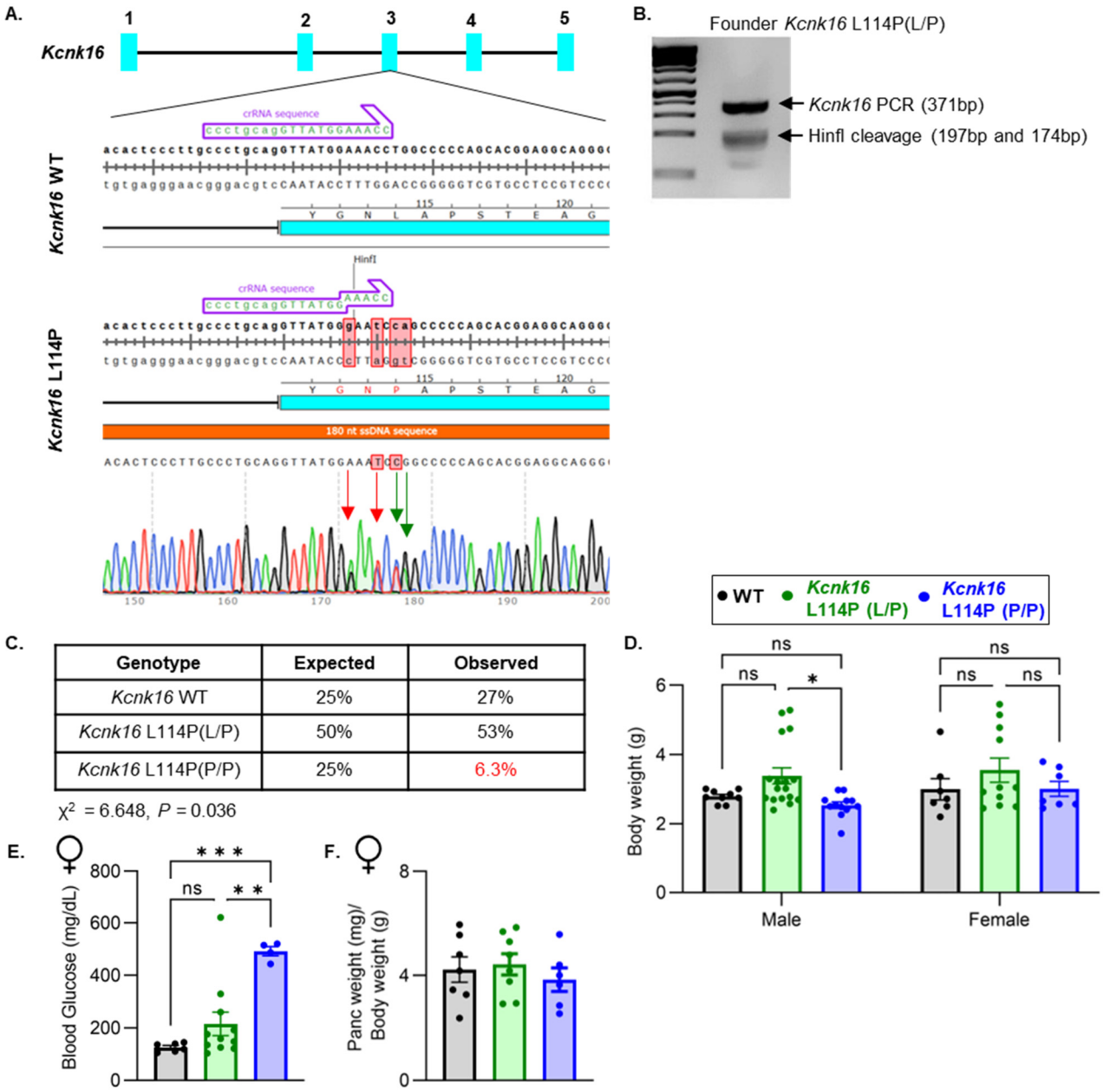


| Genotype | Expected | Observed |
|---|---|---|
| *Kcnk16* WT | 25% | 27% |
| *Kcnk16* L114P(L/P) | 50% | 53% |
| *Kcnk16* L114P(P/P) | 25% | 6.3% |

$\chi^2 = 6.648$, $P = 0.036$

**Supplemental figure 1. Generation of *Kcnk16* L114P model and assessment of neonatal glucose homeostasis and lethality. A.** Targeted region of *Kcnk16* exon 3 using CRISPR/Cas9 leading to the introduction of HinfI restriction enzyme site (red arrows) and CTG to CCA mutation in codon 337 corresponding to p.TALK-1 L114P (green arrows). **B.** PCR confirmation of the male founder *Kcnk16* L114P (L/P) mouse using HinfI

restriction digestion. **C.** $\chi^2$ analysis of the F1 progeny from B6; CD-1 *Kcnk16* L114P (L/P) crosses. **D.** Body weight measurements of male (left) and female (right) wildtype (WT; black), heterozygous *Kcnk16* L114P (L/P; green), and homozygous *Kcnk16* L114P (P/P; blue) mice on P4. **E.** Blood glucose measurements of female mice on P4. **F.** Pancreas weight/ body weight measurements of P4 female mice. Data are presented as mean±SEM. Data were analyzed using student's t-test or one-way ANOVA.

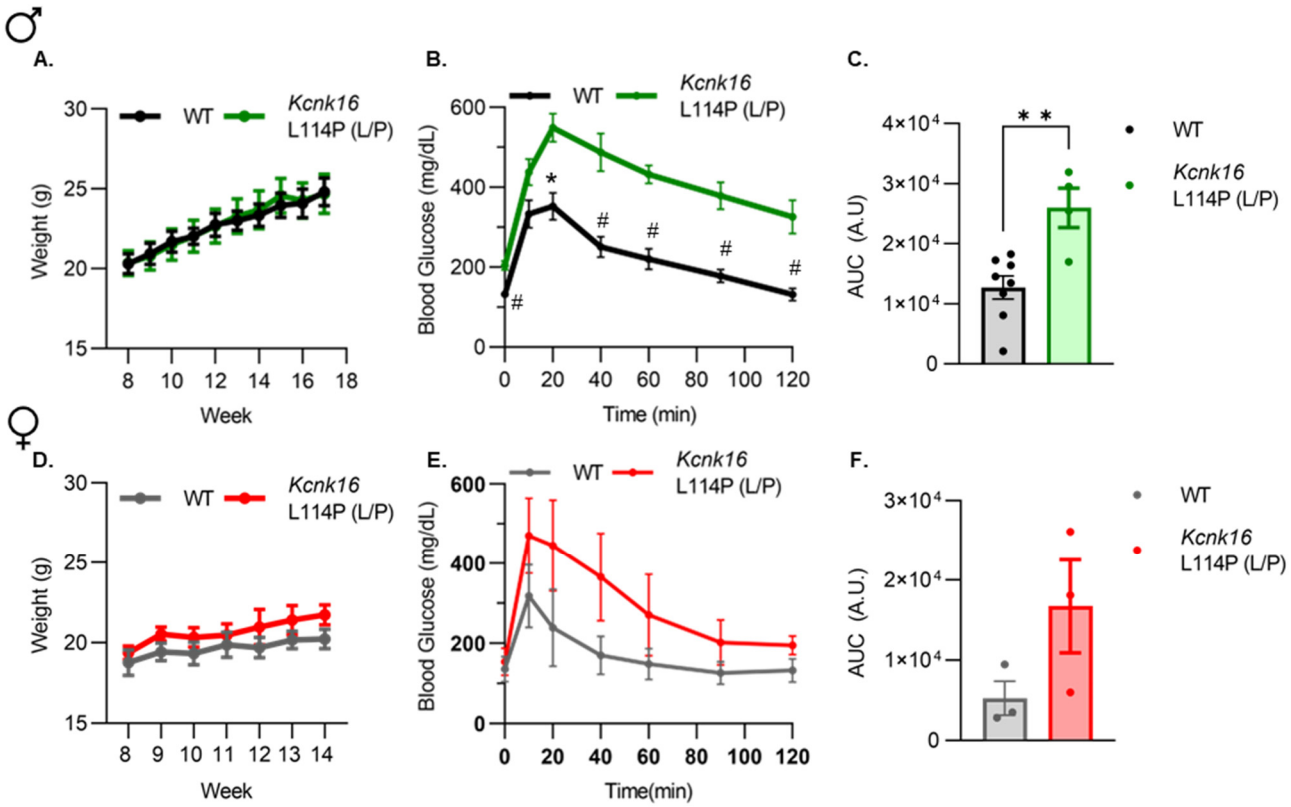


**Supplemental figure 2. Glucose homeostasis is also impaired in the *Kcnk16* L114P (L/P) mice in the B6 background. A.** Body weight measurements of male WT (black; N=8) and *Kcnk16* L114P (L/P; green; N=4) mice in the C57Bl/6J background. **B.** Intraperitoneal glucose tolerance test (i.p. GTT) performed in 10-week-old male mice following a 4-hour fast in response to 2mg/g glucose injection. **C.** Average AUC of the 2-hr GTT excursion profiles in (**c**). **D.** Body weight measurements of female WT (gray; N=3) and *Kcnk16* L114P (L/P; red; N=3) mice. **E.** I.P. GTT performed in 11-week-old female mice following a 4-hour fast in response to 2mg/g glucose injection. **F.** Average AUC of the 2-hr GTT excursion profiles in (**E**). Data are presented as mean±SEM. Data were analyzed using student's t-test; **P<0.01, #P<0.001.

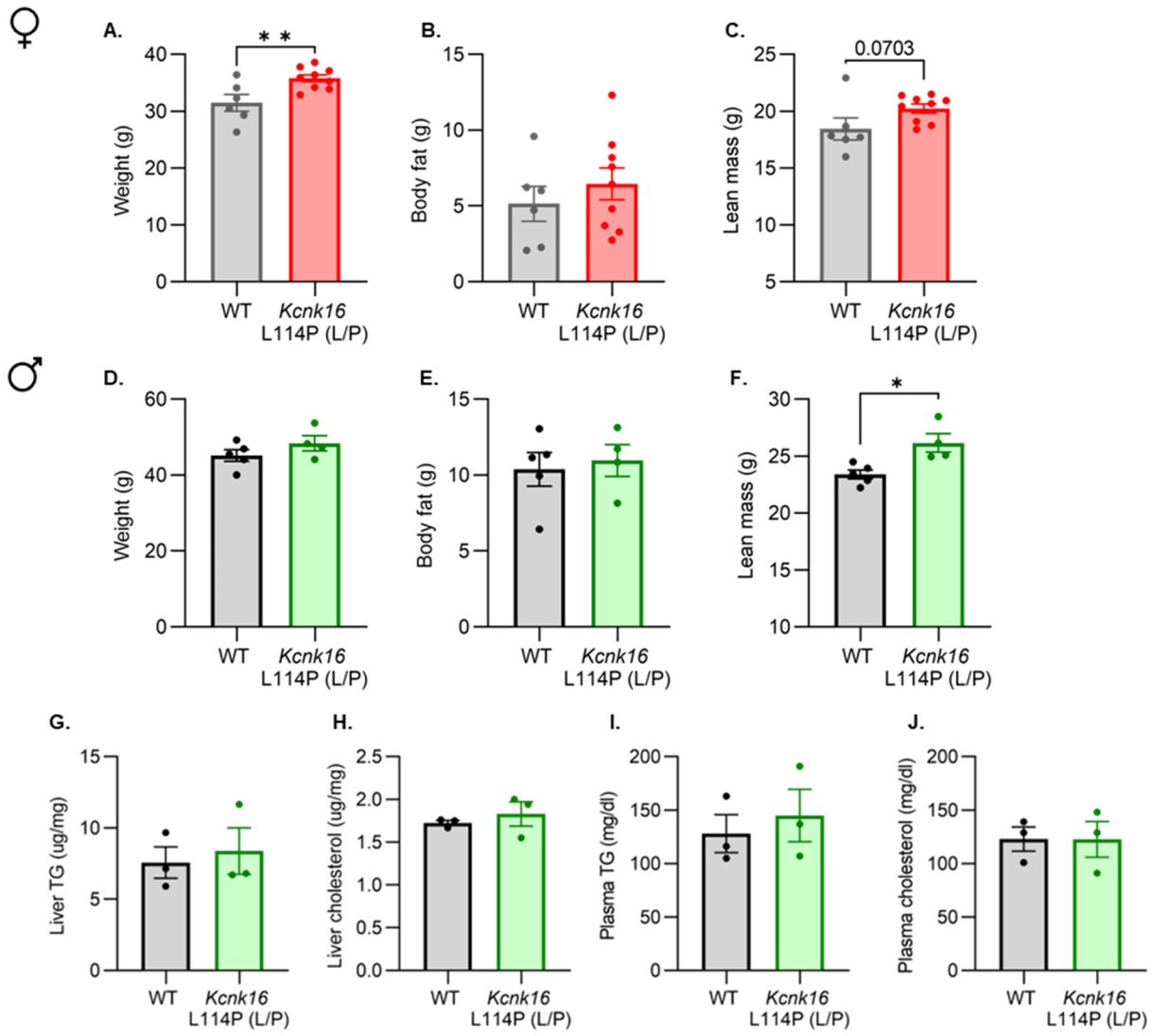


**Supplemental figure 3. Body composition measurements and assessment of plasma and liver triglycerides and total cholesterol. A.-F.** Body composition analysis of male and female B6; CD-1 WT and *Kcnk16* L114P (L/P) mice assessing weight (g), body fat (g), and lean mass (g) (N=5-9 mice/genotype). **G.-J.** Average liver and plasma cholesterol and triglyceride levels in male B6; CD-1 WT and *Kcnk16* L114P (L/P) mice (N=3/genotype). Data are presented as mean±SEM. Data were analyzed using student's t-test.

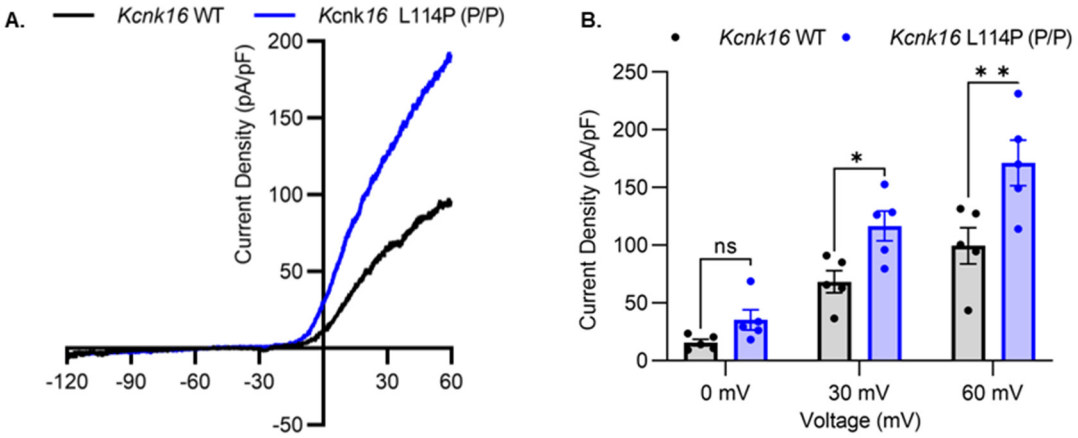


**Supplemental figure 4. K2P currents in β-cells from homozygous *Kcnk16* L114P (P/P) mice also exhibit a modest increase. A.** Representative whole-cell K2P current density (pA/pF) recorded using a voltage ramp (-120 mV to +60 mV) in 11 mM G in islets from B6; CD-1 WT and *Kcnk16* L114P (P/P) P4 neonates. B. Average current density (pA/pF) measured at the specified membrane potentials (N=5 cells/genotype). Data are presented as mean±SEM. Data were analyzed using two-way ANOVA.

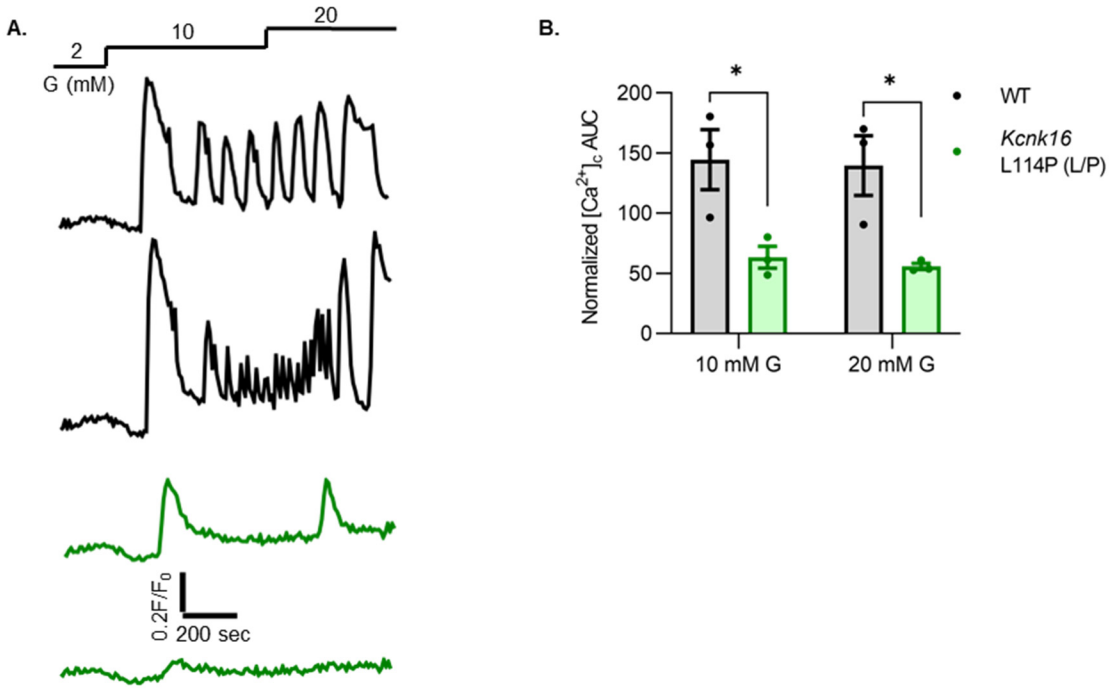


**Supplemental figure 5. Islets from *Kcnk16* L114P (L/P) mice on the B6 background also exhibit blunted glucose-stimulated $Ca^{2+}$ entry. A.** Representative GSCI traces in islets from male WT and *Kcnk16* L114P(L/P) mice in the C57BL/6J background in response to 2 mM G, 10 mM G, and 20 mM G (N=3 mice/genotype). **B.** Average total AUC in response to the indicated glucose concentrations in islets from male WT and *Kcnk16* L114P(L/P) mice. Data are presented as mean±SEM. Data are analyzed using student's t-test.

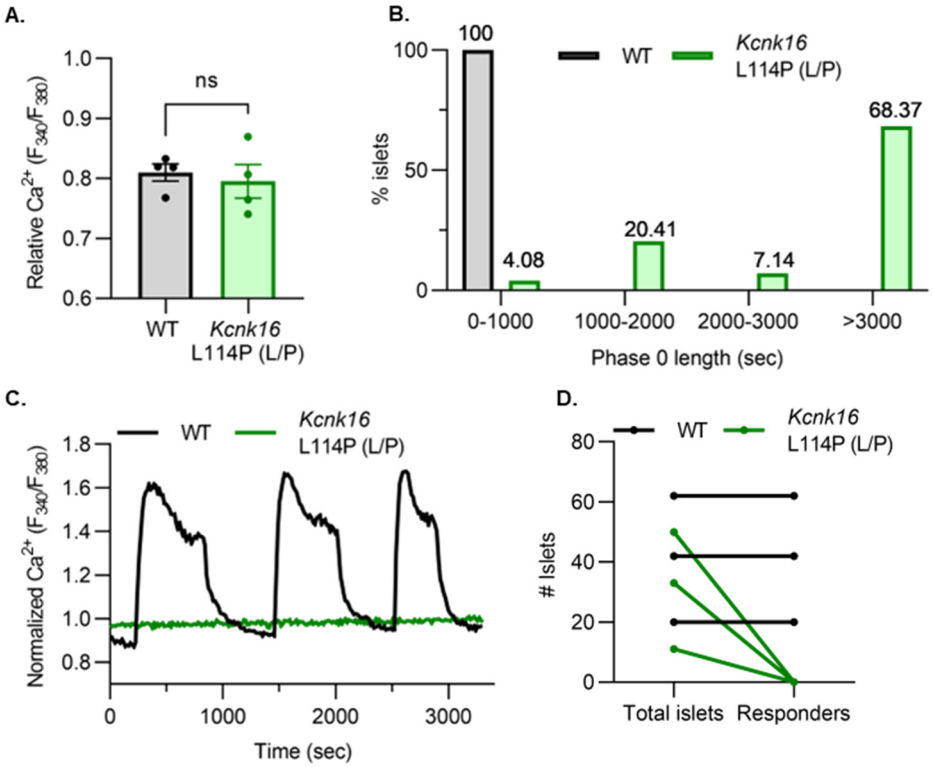


**Supplemental figure 6. *Kcnk16* L114P (L/P) islets exhibit prolonged glucose-stimulated phase 0 $[Ca^{2+}]_{ER}$ uptake and show a complete absence of $Ca^{2+}$ oscillations. A.** Average relative $[Ca^{2+}]_c$ at 2 mM G in islets from B6; CD-1 WT and *Kcnk16* L114P (L/P) mice (N=4 mice/genotype). **B.** Percent islets that exhibit the corresponding phase 0 response length (sec) in WT and *Kcnk16* L114P (L/P) mice. **C.** Representative glucose-stimulated $[Ca^{2+}]_c$ oscillations recorded at 9 mM G in islets from WT and *Kcnk16* L114P (L/P) mice. **D.** Total number of islets analyzed for $[Ca^{2+}]_c$ oscillations vs. the number of islets that exhibited $[Ca^{2+}]_c$ oscillations from WT and *Kcnk16* L114P (L/P) mice (N=3 mice/genotype). Data are presented as mean±SEM. Data are analyzed using student's t-test.

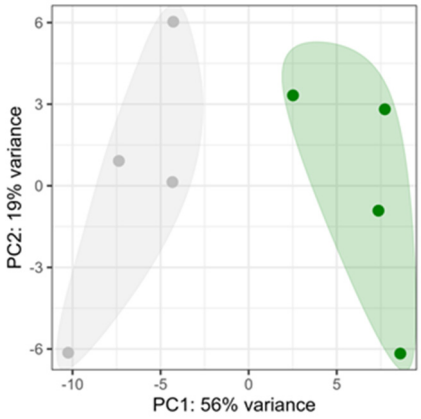


**Supplemental figure 7. Principal component analysis (PCA) showing clustering of WT (gray) and *Kcnk16* L114P (L/P; green) islet RNA samples.**

| Gene | Forward primer | Reverse primer |
|---|---|---|
| *18sRNA* | GTAACCCGTTGAACCCCATT | CCATCCAATCGGTAGTAGCG |
| *Cacna1g* | GAGACACAGAGTACGGGAGC | CAGGCATTTCATGGTCAGCG |
| *Sst* | CCACCGGGAAACAGGAACTG | TTGCTGGGTTCGAGTTGGC |
| *Asb11* | TGGTGGACTGTCAGACTGCT | ATTGACGTTGATGCCTTGCG |
| *Fxyd3* | ACTCTGCTTTCTCCCGGAAC | CTCGGAGGCTGTACCAATCATA |
| *Aldh1a3* | GGGTCACACTGGAGCTAGGA | CTGGCCTCTTCTTGGCGAA |
| *Camk1d* | CCGCCCTACAGCATTAGTCT | GAAAAGGCCCCAGTTCCGA |
| *Cxcl1* | ACCCAAACCGAAGTCATAGCC | TTGTCAGAAGCCAGCGTTCA |
| *Adcyap1r1* | CTGCGTGCAGAAATGCTACTG | AGCCGTAGAGTAATGGTGGATAG |
| *Aldob* | AGAAGGACAGCCAGGGAAAT | GTTCAGAGAGGCCATCAAGC |
| *Pdk4* | TGGTAGCAGTAGTCCAAGATGC | GTGGATTGGTTGGCCTGGAA |
| *Tgfb2* | TCGACATGGATCAGTTTATGCG | CCCTGGTACTGTTGTAGATGGA |

**Supplemental table 1. Mouse primer sequences used for qRT-PCR.**